Analysis of Photobleaching in Single-Molecule Multicolor Excitation and Förster Resonance Energy Transfer Measurements †

ARTICLE *in* THE JOURNAL OF PHYSICAL CHEMISTRY A · APRIL 2006

Impact Factor: 2.69 · DOI: 10.1021/jp054581w · Source: PubMed

6 AUTHORS, INCLUDING:

Jerker Widengren
KTH Royal Institute of Technology
108 PUBLICATIONS **3,966** CITATIONS
SEE PROFILE

Suren Felekyan
Heinrich-Heine-Universität Düsseldorf
51 PUBLICATIONS **1,688** CITATIONS
SEE PROFILE

Claus A M Seidel
Heinrich-Heine-Universität Düsseldorf
133 PUBLICATIONS **5,735** CITATIONS
SEE PROFILE

Analysis of Photobleaching in Single-Molecule Multicolor Excitation and Förster Resonance Energy Transfer Measurements†

Christian Eggeling,*,‡ Jerker Widengren,§ Leif Brand,|| Jörg Schaffer,⊥ Suren Felekyan,# and Claus A. M. Seidel*,#

Department of NanoBiophotonics, Max-Planck-Institute for Biophysical Chemistry, Am Fassberg 11, 37077 Göttingen, Germany, Royal Institute of Technology, AlbaNova University Center, Experimental Biomolecular Physics, 10691 Stockholm, Sweden, Future Technologies Division, VDI Technologiezentrum GmbH, Graf-Recke-Str. 84, 40239 Düsseldorf, Germany, Carl Zeiss AG, Development Light Microscopy, Königsallee 9-21, 37081 Göttingen, Germany, and Lehrstuhl für Molekulare Physikalische Chemie, Heinrich-Heine-University Düsseldorf, Universitätsstrasse 1, 40225 Düsseldorf, Germany

Received: August 15, 2005; In Final Form: January 12, 2006

Dye photobleaching is a major constraint of fluorescence readout within a range of applications. In this study, we investigated the influence of photobleaching in fluorescence experiments applying multicolor laser as well as Förster resonance energy transfer (FRET) mediated excitation using several red-emitting dyes frequently used in multicolor experiments or as FRET acceptors. The chosen dyes (cyanine 5 (Cy5), MR121, Alexa660, Alexa680, Atto647N, Atto655) have chemically distinct chromophore systems and can be excited at 650 nm. Several fluorescence analysis techniques have been applied to detect photobleaching and to disclose the underlying photophysics, all of which are based on single-molecule detection: (1) fluorescence correlation spectroscopy (FCS) of bulk solutions, (2) fluorescence cross-correlation of single-molecule trajectories, and (3) multiparameter fluorescence detection (MFD) of single-molecule events. The maximum achievable fluorescence signals as well as the survival times of the red dyes were markedly reduced under additional laser irradiation in the range of 500 nm. Particularly at excitation levels at or close to saturation, the 500 nm irradiation effectively induced transitions to higher excited electronic states on already excited dye molecules, leading to a pronounced bleaching reactivity. A theoretical model for the observed laser irradiance dependence of the fluorescence brightness of a Cy5 FRET acceptor dye has been developed introducing the full description of the underlying photophysics. The model takes into account acceptor as well as donor photobleaching from higher excited electronic states, population of triplet states, and energy transfer to both the ground and excited states of the acceptor dye. Also, photoinduced reverse intersystem crossing via higher excited triplet states is included, which was found to be very efficient for Cy5 attached to DNA. Comparing continuous wave (cw) and pulsed donor excitation, a strong enhancement of acceptor photobleaching by a factor of 5 was observed for the latter. Thus, in the case of fluorescence experiments utilizing multicolor pulsed laser excitation, the application of the appropriate timing of synchronized green and red laser pulses in an alternating excitation mode can circumvent excessive photobleaching. Moreover, important new single-molecule analysis diagnosis tools are presented: (1) For the case of excessive acceptor photobleaching, cross-correlation analysis of single-molecule trajectories of the fluorescence signal detected in the donor and acceptor detection channels and vice versa shows an anticorrelated exponential decay and growth, respectively. (2) The time difference, $T_g - T_r$, of the mean observation times of all photons detected for the donor and acceptor detection channels within a single-molecule fluorescence burst allows one to identify and exclude molecules with an event of acceptor photobleaching. The presented single-molecule analysis methods can be constrained to, for example, FRET-active subpopulations, reducing bias from FRET-inactive molecules. The observations made are of strong relevance for and demand a careful choice of laser action in multicolor and FRET experiments, in particular when performed at or close to saturation.

Introduction

Recent years have witnessed a strongly increased number of biological, physical, and chemical applications based on fluorescence detection. Due to the superior sensitivity to environmental properties as well as its multidimensionality, that is, its ability to provide various simultaneous readouts (e.g., intensity, anisotropy, lifetime, and spectral characteristics), fluorescence-based detection has developed into one of the most important tool categories in life science.[1] Recent technological developments have enabled an ultimate sensitivity in fluorescence detection, including the possibility to observe and analyze single fluorescent molecules.[2−12] Thereby, molecular properties otherwise hidden by ensemble averaging can be revealed. The

† Part of the special issue "Jürgen Troe Festschrift".

* To whom correspondence should be addressed. E-mail: ceggeli@gwdg.de (C.E.); cseidel@gwdg.de (C.A.M.S.).

‡ Max-Planck-Institute for Biophysical Chemistry.

§ AlbaNova University Center.

|| VDI Technologiezentrum GmbH.

⊥ Carl Zeiss AG.

Heinrich-Heine-University Düsseldorf.

10.1021/jp054581w CCC: $33.50
Published on Web 02/16/2006

benefits of a single-molecule perspective have been taken advantage of in many applications, ranging from observations in solids and solutions to live-cell imaging. To go beyond mere localization of a molecule in a three-dimensional space, the single molecules under study are often characterized not only with respect to intrinsic molecular parameters such as the fluorescence lifetime and anisotropy but also with respect to information from the fluctuations of the determined parameters.[13] This information can often contain substantial additional and complementary information about, for example, molecular properties, mobilities, interactions, and dynamics. Fluorescence correlation spectroscopy (FCS),[14] burst-size distribution analysis,[15] photon count histogram (PCH) analysis,[16] and fluorescence intensity distribution analysis (FIDA)[17] belong among the most prominent fluorescence fluctuation spectroscopies. FCS is based on the analysis of fluorescence fluctuations in time, while PCH and FIDA are based on fluctuating amplitude analysis. Further development of FCS, FIDA, and PCH resulted in their multicolor successors fluorescence cross-correlation spectroscopy (FCCS)[18] and two-dimensional FIDA or PCH.[19,20]

An ultimate development in single-molecule spectroscopy is represented by single-molecule multiparameter fluorescence detection (MFD), which in addition to the spatial information permits the simultaneous collection of all traditional fluorescence parameters, that is, intensity, lifetime, and anisotropy in two or more spectral ranges.[21,22] Multiparameter single-molecule analysis makes it possible to establish two- or even multidimensional fluorescence parameter histograms, for example, of fluorescence brightness, lifetime, anisotropy, or spectral information.[23−31] Such multidimensional histograms enable the exposure, sorting, and specific selective analyses of different subpopulations within a heterogeneous sample[22,24,28−32] and have been successfully applied to study the structure and function of biomolecules in high detail.[29,30,33] Similarly, for more robust and high-throughput applications, direct fitting of such histograms has been accomplished by 2D-FIDA,[19] two-color PCH,[20] or photon arrival-time interval distribution (PAID).[34]

The latter techniques as well as MFD provide good examples of the virtues in single-molecule and fluctuation studies of applying two or more fluorescence labels emitting in different spectral ranges. For example, monitoring the coincidence of multiple fluorescence colors in space or time can unravel binding, transport, and localization events with high specificity and in large detail.[18,19] As a multicolor method, Förster resonance energy transfer (FRET)[35] provides a sensitive tool for measuring inter- and intramolecular distances and distance changes in a range of 1−10 nm. FRET makes use of two labels, a donor and an acceptor, where the excitation of the donor dye can result in acceptor fluorescence emission due to a transfer of the donor's energy to the acceptor. The efficiency of the energy transfer and thus the amount of fluorescence emitted by the acceptor dye strongly depends on the distance between the two dyes. The transfer efficiency also depends on characteristics such as the spectral overlap and the orientation of the two labels. A large number of life science applications are based on FRET,[27,36−41] and FRET has also been combined with fluorescence fluctuation spectroscopy[42−44] and single-molecule spectroscopy.[29−32,39,45] In the latter case, methods such as MFD disclose different molecular states based on their specific FRET efficiencies.[29,30] Additionally, application of *a*lternating-*l*aser *ex*citation (ALEX) makes it possible to set up two-dimensional histograms displaying FRET efficiencies and donor and acceptor labeling degrees, distinguishing also low-FRET events from donor-only labeled species.[31] *P*ulsed *i*nterleaved *e*xcitation (PIE)[46] can reveal species with low FRET efficiencies in a similar fashion. Here, spectral cross-talk is eliminated via alternating excitation pulses of different colors, one for excitation of the donor dye and for FRET, and the other for separate excitation of the acceptor dye, respectively.

High signal levels are often important in fluorescence experiments, to acquire the necessary information content, to reach the required image scanning rates, and/or to reach the needed time resolution. This is especially pronounced for single-molecule or fluorescence fluctuation experiments, where a low signal cannot be compensated by a concentration increase of the fluorescent molecules investigated. As a consequence, high laser irradiances are often applied. However, the maximum applicable irradiance is limited by the photophysics of the dye labels, in particular by singlet and triplet saturation as well as by photobleaching. Photobleaching is to a large extent a consequence of an enhanced reactivity of the fluorophore in its excited state,[47] and it thus scales with the applied irradiance. Moreover, recent work on several dyes has shown that even for continuous wave (cw) excitation and in particular for short-pulsed laser excitation, photobleaching is severely enhanced due to the population of higher excited electronic states.[48,49] In polar solvents such as water, these states couple quite efficiently with ionic states, leading to a pronounced reactivity.[50,51] This nonlinear dependence on the applied irradiance requires well-chosen experimental conditions with respect to laser irradiance and pulse length. Eventually, optimal conditions are a tradeoff between maximum observation time, maximum photon number, and minimized (heterogeneous) photobleaching. Nonetheless, this optimization is crucial and is strongly facilitated by detailed knowledge of the relevant photophysical mechanisms.

In this work, we focus on characterizing the photobleaching in two-color and FRET experiments, where laser light either of several wavelengths and/or of a wavelength not usually employed can generate additional photophysical transitions within the dyes. For example, in most FRET experiments, laser light of only one wavelength is required for both, direct excitation of the donor and FRET-mediated excitation of the acceptor dye. However, effects from direct irradiation at this wavelength often have to be taken into consideration also for the acceptor dye, although the laser light does not excite the acceptor directly, at least not from its ground state. This also holds true for multicolor experiments, where several different dye labels and laser wavelengths are employed simultaneously. Some FRET imaging techniques, such as *p*hoto*b*leaching FRET (*pb*FRET), even directly exploit the specific photodestruction of donor or acceptor dyes to gain more spatial information on molecular distributions and mobilities in cells.[52−54] However, as in most fluorescence experiments, photobleaching of either dye is unwanted, since it usually leads to limited and biased results.[43,47−49,55,56] Recently, photodestruction-intermediate states of a FRET acceptor have been reported, which are nonemitting but still able to quench the fluorescence of the donor.[57] On the other hand, the sensitivity of the red-excited and red-emitting dye cyanine 5 (Cy5) to green light has also been reported. In these experiments in deoxygenated aqueous solutions and with added triplet quencher, excitation at 633 nm drove the dye into a nonfluorescent, quasi-photobleached state, while addition of green light at around 500 nm led to recovery of the Cy5 fluorescence, turning Cy5 into an optical switch.[58,59] In view of these seemingly contradictive results, the overall importance of dye photobleaching, and the additional effects observed under multiwavelength and FRET-mediated excitation, a more detailed and general understanding of the photobleaching impact of green

light for red-emitting dyes is needed, as is the development of methods providing remedies to these photobleaching effects.

In this study, the photobleaching properties of several red-emitting dyes with chemically distinct chromophore systems, Cy5, MR121, Alexa660, Alexa680, Atto647N, and Atto655, and of a Cy5 FRET conjugate were investigated in solution at simultaneous or separate green and red laser excitation using FCS and single-molecule analysis methods. The dyes belong to various classes of, for example, oxazine, carbopyronine, or cyanine chromophores. Especially Alexa660 and 680 show very broad absorption spectra and are expected to be distinct from the other dyes. It is outlined how extensive photobleaching by the green laser light, interacting with the excited states of the dyes, limits the maximum accessible fluorescence brightness. A clear distinction between the cw and pulsed excitation modes can be observed, and the features of photobleaching with respect to the population of the triplet state and of higher excited electronic states, energy transfer to the acceptor's ground and excited states, as well as photoinduced reverse intersystem crossing via higher excited triplet states are considered. The presented results are to a great extent only accessible by single-molecule fluorescence analysis. They reveal major limitations in multicolor and FRET experiments that can be attributed to enhanced photobleaching of the acceptor dye. On the basis of the findings, optimal experimental conditions with respect to fluorescence output and minimized photobleaching in terms of laser irradiance, excitation mode, and pulse synchronization of different laser wavelengths are outlined. Moreover, readily accessible new single-molecule analysis methods are presented to check for the amount of photobleaching, providing adequate guidance for the proper optimization adjustments: (1) For the case of excessive acceptor photobleaching, cross-correlation analysis of single-molecule trajectories of the fluorescence signal detected in the donor and acceptor detection channels and vice versa shows an anticorrelated exponential decay and growth, respectively. (2) The time difference, $T_g - T_r$, of the mean observation times of all photons detected for the donor and acceptor detection channels within a single-molecule fluorescence burst allows one to identify and exclude molecules with an event of acceptor photobleaching. In this way, various single-molecule analysis methods presented above can be constrained to, for example, FRET-active subpopulations, reducing bias from FRET-inactive molecules.

Theory

The theoretical part introduces the photokinetic model of photobleaching in two-color and FRET experiments. The first part gives a general theoretical characterization of the fluorescence emission of a dye regarding photobleaching. In the second part, this theoretical description is extended to Förster resonance energy transfer (FRET) experiments.

General Photokinetic Model of Photobleaching for Direct One- or Two-Color Excitation. Figure 1A depicts the general photophysical model of photobleaching of a dye, based on five electronic levels: the singlet ground state, S_0, the first excited singlet state, S_1, the lowest triplet state, T_1, and higher excited singlet and triplet states, S_n and T_n. Vibrational substates can be disregarded due to their comparatively short lifetime. The kinetic rate constants underlying the possible transitions between the electronic states are denoted as follows: k_{01}, excitation from S_0 to S_1; k_{10}, sum of all processes leading to the de-excitation of S_1 to S_0 (i.e., internal conversion, k_{IC}, fluorescence, k_f); k_{ISC}, intersystem crossing (ISC) from S_1 to T_1; k_T, rate of back ISC from T_1 to S_0 (inverse triplet lifetime); k_{S1n} and k_{T1n}, excitation from S_1 to S_n or T_1 to T_n, respectively; k_{Sn1} and k_{Tn1}, de-excitation of S_n and T_n to S_1 and T_1, respectively; and k^*_{ISC} and k^*_{ReISC}, crossing between T_n and S_n, that is, photoinduced ISC and reverse ISC. Photobleaching reactions occur from S_1, T_1, S_n, and T_n and are accounted for by the rate constants k_{bS1}, k_{bT1}, k^*_{bSn}, and k^*_{bTn}, respectively. The sum of all depopulation processes of S_1, $k_0 = k_{ISC} + k_{IC} + k_f$, gives the inverse fluorescence lifetime, τ^{-1}.

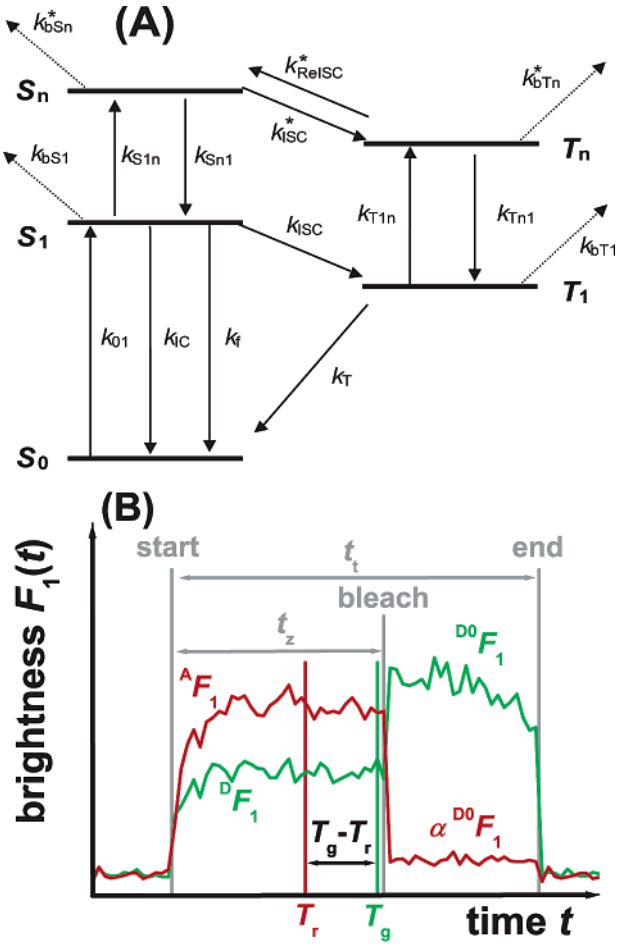

Figure 1. Photokinetic model of photobleaching. (A) Energy diagram of a dye molecule including five electronic levels and their transition rate constants. For details, see text. (B) Simulated single-molecule time trajectory of the fluorescence brightness, $F_1(t)$, in the donor channel (green line) and in the acceptor channel (red line) over time, t, exemplified for the event of acceptor photobleaching. $^{D}F_1$ (donor brightness in the presence of FRET) and $^{A}F_1$ (acceptor brightness) depict the respective values of brightness before the photobleaching event, and $^{D0}F_1$ (donor brightness in the absence of FRET) and $\alpha\ ^{D0}F_1$ (cross-talk of donor fluorescence into the acceptor detection channel) depict the respective values of brightness after the photobleaching event. "Start" and "end" denote the beginning and the end of the single-molecule transit through the detection volume, and "bleach" denotes the incident of the acceptor photobleaching. The time t_z represents the average time before photobleaching, given by $t_z = 1/^{A}k_z$ (eq 6), and the time t_t represents the average transit time of a single molecule through the detection volume. The parameters T_g and T_r exemplify the medial time of fluorescence emission of both detection channels, as used for the $T_g - T_r$ analysis in Figure 6.

The rate constants for excitation to S_1, S_n, and T_n involve the absorption of a photon and thus depend on the applied laser irradiance, I.

$$k_X(t) = \sigma_X(\lambda)\,\gamma I(t) \qquad (X = 01, S1n, T1n) \qquad (1)$$

$\sigma_{01}(\lambda)$, $\sigma_{S1n}(\lambda)$, and $\sigma_{T1n}(\lambda)$ are the corresponding absorption

cross sections, λ is the excitation wavelength, and $\gamma = \lambda/(hc_l)$ is the reciprocal photon energy, with h being Planck's constant and c_l being the velocity of light. I and σ_X are given in units of watts per square centimeter and square centimeters, respectively. The time, t, dependence of $k_X(t)$ results from $I(t)$, which is constant for continuous wave (cw) excitation and follows the pulse shape and the repetition rate in the case of pulsed excitation.

Those processes that involve the excitation to the higher excited electronic states, S_n and T_n, that is, photoinduced ISC and reverse ISC and photobleaching, can be expressed by composite rate constants starting from S_1 and T_1, introducing effective cross sections, $\sigma_{\text{ISC-}n}$, $\sigma_{\text{ReISC-}n}$, and $\sigma_{\text{b}Xn}$ and, given in $\text{cm}^2\ \text{W}^{-1}\ \text{s}^{-1}$.

$$\text{photoinduced ISC: } k_{\text{ISC-}n}(t) = (\sigma_{S1n}\gamma I(t))\phi_{\text{ISC-}n} = \sigma_{\text{ISC-}n}I(t)$$

$$\text{photoinduced reverse ISC: } k_{\text{ReISC-}n}(t) = (\sigma_{T1n}\gamma I(t))\phi_{\text{ReISC-}n} = \sigma_{\text{ReISC-}n}I(t)$$

$$\text{photobleaching, } X = S \text{ or } T\text{: } k_{\text{b}Xn}(t) = (\sigma_{X1n}\gamma I(t))\phi_{\text{b}Xn} = \sigma_{\text{b}Xn}I(t) \quad (2)$$

The parameters σ_{X1n} are the previously defined absorption cross sections for excitation from S_1 to S_n ($X = S$) and T_1 to T_n ($X = T$) (eq 1), and $\phi_{\text{ISC-}n} = k^*_{\text{ISC}}/k_{Sn1}$, $\phi_{\text{ReISC-}n} = k^*_{\text{ReISC}}/k_{Tn1}$, and $\phi_{\text{b}Xn} = k^*_{\text{b}Xn}/k_{Xn1}$ are the quantum yields for ISC, reverse ISC, and photobleaching from S_n and T_n.

By introducing these effective cross sections (eq 2), the populations of the higher excited states do not need to be explicitly calculated. This is allowed, since these states have a comparatively low lifetime of $k_{Sn1}{}^{-1}$, $k_{Tn1}{}^{-1}$ < picoseconds.[48] This leaves us with a rate equation system involving only three electronic states: the singlet ground, first excited singlet, and lowest triplet states.

$$\dot{S}_0(t) = -k_{01}(t)S_0 + k_{10}S_1 + k_T T_1 \quad (3)$$

$$\dot{S}_1(t) = k_{01}(t)S_0 - [k_{10}(t) + k_{\text{ISC}} + k_{\text{ISC-}n}(t) + k_{\text{bS1}} + k_{\text{bS}n}(t)]S_1 + k_{\text{ReISC-}n}(t)T_1$$

$$\dot{T}_1(t) = [k_{\text{ISC}} + k_{\text{ISC-}n}(t)]S_1 - [k_T + k_{\text{ReISC-}n}(t) + k_{\text{bT1}} + k_{\text{bT}n}(t)]T_1$$

The time-dependent populations of each electronic level can be calculated by solving the rate equation system for a given time course of the irradiance, $I(t)$ (compare eqs 1 and 2), and with initial populations of $S_0(0) = 1$ and $S_1(0) = T_1(0) = 0$. The calculation of $S_1(t)$ on the other hand allows for the quantification of the fluorescence brightness, $F_1(t) = \Psi\Phi\tau^{-1}S_1(t)$, which expresses the average count rate detected for a single dye molecule. Ψ denotes the fluorescence detection efficiency of the experimental setup and Φ the fluorescence quantum yield of the dye.

In the case of pulsed excitation with repetition rate υ, the brightness is given by the populations in the S_1 state after the ith excitation pulse, $S_1(i)$.[49]

$$F_1 = \Psi\Phi\sum_i^{n_P} S_1(i)/\Delta t \qquad (\text{with } n_P = \Delta t\upsilon) \quad (4)$$

Here, Δt denotes the observation time window and $n_P = \Delta t\upsilon$ the number of laser pulses within Δt. n_P amounts to about 20 580 pulses for the present experimental conditions of $\Delta t \approx 0.28$ ms and $\upsilon = 73.5$ MHz. As shown previously,[49] for simplification, a rectangular pulse shape with the experimentally determined width of in this case 180 ps can be assumed.

For cw excitation, a more simple approach can be used, applying the steady state populations of the first excited singlet state, $S_{1\text{eq}}$, and of the lowest triplet state, $T_{1\text{eq}}$, deduced from eq 3.

$$S_{1\text{eq}} = \frac{k_{01}(k_T + k_{\text{ReISC-}n})}{k_{01}(k_T + k_{\text{ISC}} + k_{\text{ISC-}n} + k_{\text{ReISC-}n}) + k_{10}(k_T + k_{\text{ReISC-}n}) + k_T(k_{\text{ISC}} + k_{\text{ISC-}n})}$$

$$T_{1\text{eq}} = (k_{\text{ISC}} + k_{\text{ISC-}n})/(k_T + k_{\text{ReISC-}n})S_{1\text{eq}} \quad (5)$$

Photobleaching can be constituted into this steady state approach by an effective bleaching rate constant, k_z, and the probability, $p_{\text{intact}}(t)$, of still being fluorescent after time t.[48,49]

$$k_z = (k_{\text{bS1}} + k_{\text{bS}n})S_{1\text{eq}} + (k_{\text{bT1}} + k_{\text{bT}n})T_{1\text{eq}} = [k^{\text{eff}}_{\text{b1}} + \sigma^{\text{eff}}_{\text{b}n}I(t)]S_{1\text{eq}}$$

$$p_{\text{intact}}(t) = \exp(-k_z t) \quad (6)$$

with

$$k^{\text{eff}}_{\text{b1}} = [1 + (k_{\text{ISC}} + k_{\text{ISC-}n})/(k_T + k_{\text{ReISC-}n})]k_{\text{b}X1}$$

$$\sigma^{\text{eff}}_{\text{b}n} = [1 + (k_{\text{ISC}} + k_{\text{ISC-}n})/(k_T + k_{\text{ReISC-}n})]\sigma_{\text{b}Xn}$$

$k_{\text{b}X1}$ is the rate constant of photobleaching from S_1 and T_1, while $k_{\text{b}Xn} = \sigma_{\text{b}Xn}I(t)$ depends on the irradiance, $I(t)$, and represents the composite rate constant of higher-order photobleaching via S_n and T_n (eq 2). In our experiments, the rate constants, $k_{\text{b}X1}$ and $k_{\text{b}Xn}$, cannot be assigned to specifically belong to either the singlet system ($X = S$) or the triplet system ($X = T$) and are therefore, for simplification, assumed to have the same magnitude for $X = S$ or T. This simplification introduces the effective rate constant of first-order photobleaching, $k^{\text{eff}}_{\text{b1}}$, and the effective cross section of higher-order photobleaching, $\sigma^{\text{eff}}_{\text{b}n}$, after the incident of excitation to S_1.

The average brightness, F_1, within the observation time window, Δt, is in the case of cw excitation thus given by eq 7.

$$F_1 = \Psi\Phi\tau^{-1}S_{1\text{eq}}\frac{1}{k_z\Delta t}[1 - \exp(-k_z\Delta t)] \quad (7)$$

For a single molecule diffusing through the focal observation volume, the observation time window is given by the mean transit time, $\Delta t = t_t$.

Photobleaching in Förster Resonance Energy Transfer (FRET) Experiments. FRET defines the dipole−dipole, nonradiative energy transfer from an excited dye molecule, D* (donor), to another dye molecule, A (acceptor). The energy transfer leads to the electronic excitation of the acceptor, A*, and the de-excitation of the donor, $\text{D}^* + \text{A} \rightarrow \text{D} + \text{A}^*$.[35] Thus, a bichromophoric system of donor and acceptor dye has to be considered. To distinguish between donor and acceptor, each dye is denoted by the index "D" or "A" throughout. In our case, we distinguish between three different energy transfer mechanisms: energy transfer from the donor's first excited singlet state, ${}^{\text{D}}S_1$, to the acceptor's (i) singlet ground state, ${}^{\text{A}}S_0$, (ii) first excited singlet state, ${}^{\text{A}}S_1$, and (iii) first excited triplet state, ${}^{\text{A}}T_1$.

$$\text{(i)}\ {}^{D}S_1 + {}^{A}S_0 \xrightarrow{E_{S0}} {}^{D}S_0 + {}^{A}S_1 \qquad (8)$$

$$\text{(ii)}\ {}^{D}S_1 + {}^{A}S_1 \xrightarrow{E_{S1}} {}^{D}S_0 + {}^{A}S_n$$

$$\text{(iii)}\ {}^{D}S_1 + {}^{A}T_1 \xrightarrow{E_{T1}} {}^{D}S_0 + {}^{A}T_n$$

The three pathways correspond to competitive FRET mechanisms previously observed in single bichromophoric molecules.[60,61] Energy transfer pathways starting from the lowest triplet state or from higher excited electronic states of the donor can be neglected. Due to the lower energy of ${}^{D}T_1$ and the much lower lifetimes of ${}^{D}S_n$ and ${}^{D}T_n$ compared to ${}^{D}S_1$, energy transfer pathways starting from ${}^{D}T_1$, ${}^{D}S_n$, and ${}^{D}T_n$ are much more insufficient. In all three energy transfer pathways of eq 8, donor fluorescence is quenched and, without direct laser excitation, the corresponding excited states of the acceptor are populated. To account for this quenching of donor fluorescence, we differentiate between donor in the presence (index "D") and donor in the absence (index "D0") of FRET to an acceptor dye. Pathway i sensitizes acceptor fluorescence and is, thus, the most common energy transfer mechanism, usually desired in FRET experiments. The efficiency of each energy transfer mechanism can be defined by the energy transfer efficiencies, E_{S0}, E_{S1}, or E_{T1}.

$$E_X = \frac{k_{\text{FRET-}X}}{\sum k_{\text{FRET-}X} + {}^{D0}k_0} \qquad (X = S0, S1, T1) \qquad (9)$$

${}^{D0}k_0 = 1/\tau_{D0}$ is the inverse fluorescence lifetime of the donor in the absence of any FRET to an acceptor, and $\sum$ denotes the sum over all energy transfer pathways. The microscopic rate constants, $k_{\text{FRET-}X}$, for the energy transfer are given (a) by the spectral overlap of the donor fluorescence emission with the acceptor's ground ($X = S0$), the first excited singlet ($X = S1$), or the lowest triplet state ($X = T1$) absorption spectrum, (b) by the relative orientation of the donor and acceptor dyes, and (c) by the spatial distance, R_{DA}, between both dyes, $k_{\text{FRET-}X} \sim R_{DA}{}^{-6}$.[35] This characteristic sixth-order dependence on R_{DA} makes FRET a sensitive tool to measure distance changes, usually in a range of 1−10 nm.

Some of the previously defined rate constants (eqs 1 and 2) have to be adapted to the occurrence of FRET.

(a) donor fluorescence lifetime

$$\tau_D{}^{-1}(t) = {}^{D}k_0(t) = {}^{D0}k_0 + {}^{A}S_0(t)k_{\text{FRET-}S0} + {}^{A}S_1(t)k_{\text{FRET-}S1} + {}^{A}T_1(t)k_{\text{FRET-}T1}$$

(b) acceptor excitation rate

$${}^{A}k_{01}(t) = {}^{A}\sigma_{01}\gamma I(t) + {}^{D}S_1(t)k_{\text{FRET-}S0}$$

(c) acceptor photoinduced ISC

$${}^{A}k_{\text{ISC-}n}(t) = {}^{A}\sigma_{\text{ISC-}n}I(t) + {}^{D}S_1(t)k_{\text{FRET-}S1}{}^{A}\phi^*_{\text{ISC-}n}$$

(d) acceptor photoinduced reverse ISC

$${}^{A}k_{\text{ReISC-}n}(t) = {}^{A}\sigma_{\text{ReISC-}n}I(t) + {}^{D}S_1(t)k_{\text{FRET-}T1}{}^{A}\phi^*_{\text{ReISC-}n}$$

(e) higher-order acceptor photobleaching ($X = S$ or T)

$${}^{A}k_{bXn}(t) = {}^{A}\sigma_{bXn}I(t) + {}^{D}S_1(t)k_{\text{FRET-}X1}{}^{A}\phi^*_{bXn} \qquad (10)$$

${}^{D0}k_0 = {}^{D0}k_{10} + {}^{D}k_{ISC} = \tau_{D0}{}^{-1}$ depicts the inverse fluorescence lifetime of the donor in the absence of an energy transfer to an acceptor dye, and ${}^{A}\sigma_{01}$, the absorption cross section for direct laser light excitation of the acceptor to ${}^{A}S_1$. ${}^{A}\sigma_{01}$ is usually very low, since the wavelength of the excitation light is optimized for the donor and far away from the absorption maximum of the acceptor. ${}^{A}\sigma_{\text{ISC-}n}$, ${}^{A}\sigma_{\text{ReISC-}n}$, and ${}^{A}\sigma_{bXn}$ are the composite cross sections of the acceptor for photoinduced ISC and reverse ISC and photobleaching induced by the time-dependent irradiance, $I(t)$ (eq 2), while ${}^{A}\phi^*_{\text{ISC-}n}$, ${}^{A}\phi^*_{\text{ReISC-}n}$, and ${}^{A}\phi^*_{bXn}$ express the quantum yields for photoinduced ISC and reverse ISC and photobleaching from the higher excited states of the acceptor induced by FRET (eq 2). The asterisk marks the fact that, due to the different spectral ranges of the laser- and FRET-induced excitation, these quantum yields may differ from those defined for the corresponding processes following direct absorption of the excitation light. The latter quantum yields, ${}^{A}\phi_{\text{ISC-}n}$, ${}^{A}\phi_{\text{ReISC-}n}$, and ${}^{A}\phi_{bXn}$, are included within the composite cross sections ${}^{A}\sigma_{\text{ISC-}n}$, ${}^{A}\sigma_{\text{ReISC-}n}$, and ${}^{A}\sigma_{bXn}$ (eq 2). Due to the Stokes shift between excitation and emission of the donor, the energy of the laser light for donor excitation is higher than the energy mediated by FRET. This results in higher energy levels of ${}^{A}S_n$ and ${}^{A}T_n$ and, thus, higher efficiencies for ISC, reverse ISC, and photobleaching from these states, compared to FRET-mediated excitation.

From eq 10, a decreased fluorescence lifetime of the donor dye as well as the sensitization of acceptor fluorescence follows upon occurrence of FRET. Furthermore, eq 10 also takes into account the fact that a certain energy transfer cannot occur if any of the involved initial states are not populated. Thus, the rate of FRET scales with the population of the first excited singlet state of the donor (${}^{D}S_1(t)$) or with those of the corresponding states of the acceptor (${}^{A}S_0(t)$, ${}^{A}S_1(t)$, ${}^{A}T_1(t)$).

Full Simulation of the Donor−Acceptor System. To simulate the fluorescence signal of the bichromophoric donor−acceptor system, the population of the donor's and acceptor's first excited singlet state, ${}^{D}S_1(t)$ and ${}^{A}S_1(t)$, can be calculated by simultaneously solving the rate equation system of eq 3 for donor and acceptor dye. The complete rate equation system in the case of FRET thus includes six equations, three for each dye, which are linked via eq 10. Fluorescence emitted by the donor and acceptor is detected in two spectrally distinct detection channels. The corresponding fluorescence brightnesses, ${}^{g}F_1$ and ${}^{r}F_1$, detected in the "green" and "red" detection channels, respectively, are given by the fluorescence brightness of the donor, ${}^{D}F_1$, and of the acceptor, ${}^{A}F_1$.

$${}^{g}F_1 = {}^{D}F_1 \qquad (11)$$

$${}^{r}F_1 = {}^{A}F_1 + \alpha\, {}^{D}F_1$$

with

$${}^{D}F_1 = \Psi_g\Phi_D\tau_D{}^{-1}\,{}^{D}S_1(t) \quad \text{and} \quad {}^{A}F_1 = \Psi_r\Phi_A\tau_A{}^{-1}\,{}^{A}S_1(t)$$

Ψ_g and Ψ_r are the detection efficiencies of each detection channel, Φ_D and Φ_A are the fluorescence quantum yields, and τ_D and τ_A are the fluorescence lifetimes of donor and acceptor, respectively. The donor cross-talk, α, amounts for the fact that cross-talk between the two detection channels may occur due to fluorescence emission of the donor bleeding into the acceptor's (red) detection channel. ${}^{D}F_1$ and ${}^{A}F_1$ can be calculated from ${}^{D}S_1(t)$ and ${}^{A}S_1(t)$ corresponding to eq 4 for pulsed excitation and eq 7 for cw excitation.

Inhomogeneous Focal Volume. For a focal volume formed by an objective lens of high numerical aperture, the laser

irradiance and, thus, all irradiance-dependent rate constants strongly depend on space. The spatial dependence of the focal irradiance can be approximated by a three-dimensional Gaussian profile, $I(x,y,z) = I_0 \exp(-2(x^2 + y^2)/\omega_0^2) \exp(-2z^2/\omega_z^2)$, with the focal irradiance $I_0 = I(z = 0)$ and $1/e^2$ radii ω_0 and ω_z in radial (x, y) and axial (z) directions, respectively. To simplify expressions for photophysical processes, it is justified to approximate the excitation volume by a rectangular profile with radius ω_0. As shown before, an average rate constant, $k(I)$, can be defined in such a case, where I is given by $I_0/2$.[24,48,49,62,63]

Fluorescence Correlation Spectroscopy (FCS). The overall fluorescence signal detected from a solution of fluorescent molecules is given by the mean number of molecules in the observation volume, c, denoted concentration throughout, and by the fluorescence brightness of each single molecule, F_1 (see eqs 4 and 7); $F = c \times F_1$. Variations in c or in F_1 are caused by, for example, diffusion and chemical reaction. These variations lead to temporal fluctuations in the fluorescence signal around an average value, $F(t) = \langle F(t)\rangle + \delta F(t)$, which are analyzed in FCS by means of the second-order autocorrelation function, $G(t_c)$.[13]

$$G(t_c) = 1 + \frac{\langle \delta F(t)\, \delta F(t + t_c)\rangle}{\langle F(t)\rangle^2} \qquad (12)$$

Here, t_c represents the correlation time. Triangular brackets indicate averaging over the measurement time, t.

Irreversible photobleaching reactions to a nonfluorescent product give rise to an abrupt termination of fluorescence emission, and thus to characteristic fluorescence fluctuations. In the autocorrelation function, the abrupt termination of fluorescence emission results in an apparently shorter observation time. Because the total sample volume is much larger than the excitation volume, the depletion of fluorophores within the focus due to photobleaching will be balanced by a net in-flow from out-of-focus regions due to the formed concentration gradient. Consequently, photobleaching can be treated as a chemical pseudoequilibrium reaction using the effective bleaching rate constant, $k_z(I_0/2)$ (eq 6). In this way, the autocorrelation function taking diffusion dynamics, dark state population (such as the triplet state), and photobleaching kinetics into account can be approximated by eq 13.[48,49,62,63]

$$G(t_c) = 1 + \frac{1}{c}[G_{Diff}(t_c)\, G_B(t_c) + G_{Dark}(t_c)] \qquad (13)$$

with

$$G_{Diff}(t_c) = \left(\frac{1}{1 + t_c/\tau_{Diff}}\right)\left(\frac{1}{1 + (\omega_0/\omega_z)^2(t_c/\tau_{Diff})}\right)^{1/2} \quad \text{(diffusion)}$$

$$G_B(t_c) = 1 - A + A \exp(-k_z t_c) \quad \text{(bleaching)}$$

$$G_{Dark}(t_c) = \frac{F_D}{1 - F_D} \exp(-t_c/\tau_{Dark}) \quad \text{(dark state)}$$

The characteristic diffusion time is given via the diffusion coefficient, D, by $\tau_{Diff} = \omega_0^2/(4D)$. c is the concentration, that is, the mean number of fluorescent molecules in the detection volume, F_D denotes the equilibrium fraction of molecules in the dark state such as T_1, τ_{Dark} is the characteristic dark state correlation time, characterized by the population and depopulation kinetics, and A is an amplitude describing the average bleaching decay with rate constant k_z. While the dark state term, $G_{Dark}(t_c)$, is added, the bleaching, $G_B(t_c)$, and the diffusion terms, $G_{Diff}(t_c)$, are multiplied, since they both decay in about the same time scale.

Cross-Correlation Analysis of Acceptor Photobleaching in Single-Molecule Bursts. In the present FRET experiments, the distinct detection of donor and acceptor fluorescence in the two detection channels permits the calculation of the cross-correlation function of both signals.

$$G_{gr}(t_c) = 1 + \frac{\langle \delta^g F_1(t)\, \delta^r F_1(t + t_c)\rangle}{\langle {}^gF_1(t)\rangle\langle {}^rF_1(t)\rangle}$$

$$G_{rg}(t_c) = 1 + \frac{\langle \delta^r F_1(t)\, \delta^g F_1(t + t_c)\rangle}{\langle {}^gF_1(t)\rangle\langle {}^rF_1(t)\rangle} \qquad (14)$$

${}^gF_1$ and ${}^rF_1$ denote the fluorescence brightness detected in the donor and acceptor detection channels (eq 11). Note that, in contrast to eq 12, the cross-correlation function is in this case defined on the basis of the fluctuating fluorescence brightness, $F_1(t)$, since in the present experiments the cross-correlation analysis of the acceptor photobleaching is solely applied to time trajectories of single molecules.

The analysis of the cross-correlation function discloses processes that influence both the donor and acceptor fluorescence signals simultaneously (coincidence signal).[18] Three processes reveal concomitant variations in the fluorescence brightness of both dyes and thus influence the cross-correlation function. (1) Fast fluctuations in the microsecond time domain occur due to the population of dark states such as the triplet state of both dyes[62] or photoisomerization.[64−66] The population of a donor's dark state interrupts the energy transfer and thus the fluorescence emission of the acceptor. As discussed before (eq 8), energy transfer from the donor's dark (triplet) state is negligible. Further, the acceptor in the triplet or dark state may absorb the donor's energy in a different way as in the ground state, leading to concomitant change in donor fluorescence emission. Due to this correlated behavior, these dark state fluctuations contribute to the cross-correlation function in a similar way as the dark state term, $G_{Dark}(t_c)$, of eq 13. (2) Since both dyes are tagged to the same molecule, diffusion through the focus with a mean transit time, t_t, influences the fluorescence emission of both dyes in the same way. (3) Irreversible photobleaching of the acceptor dye makes it unable to emit fluorescence and to absorb the donor's energy. Acceptor photobleaching thus reveals an interruption of FRET accompanied by a loss of acceptor fluorescence and a concomitant rise in fluorescence brightness of the donor, exemplified in Figure 1B. This photobleaching step occurs after a time, t_z, that is on average given by the effective bleaching rate constant of the acceptor; $t_z = 1/{}^Ak_z$ (eq 6). Photodestruction-intermediate states that are nonemitting but still able to quench the fluorescence of the donor have been observed in previous single-molecule FRET experiments[57] but have not been observed in our experiments and are thus neglected.

As given in the Supporting Information, $G_{gr}(t_c)$ and $G_{rg}(t_c)$ can be approximated for the special case of $t_z \ll t_t$, that is, if photobleaching is faster than diffusion.

$$G_{gr}(t_c) = {}^{gr}B_0 + {}^{gr}B_1 \exp(-k_z t_c) + G_{Dark}(t_c) \qquad (15)$$

$$G_{rg}(t_c) = {}^{rg}B_0 - {}^{rg}B_1 \exp(-k_z t_c) + G_{Dark}(t_c)$$

with

$$^{gr}B_0 \approx \frac{\alpha\, ^{D0}F_1}{^{A}F_1}\frac{t_t}{t_z} \qquad ^{gr}B_1 \approx \frac{^{D}F_1}{^{D0}F_1}$$

$$^{rg}B_0 \approx 1 + \frac{\alpha\, ^{D0}F_1}{^{A}F_1}\frac{t_t}{t_z} \qquad ^{rg}B_1 \approx 1 - \frac{^{D}F_1}{^{D0}F_1}$$

where, according to Figure 1B, $^{D}F_1$ and $^{A}F_1$ represent the fluorescence brightness of donor and acceptor before the photobleaching event, that is, in the presence of FRET, and $^{D0}F_1$ represents the brightness of the donor after the photobleaching event, with $\alpha\, ^{D0}F_1$ being the concomitant brightness detected in the acceptor channel due to cross-talk, α. The most important criterion for photobleaching is the fact that the correlation functions $G_{gr}(t_c)$ and $G_{rg}(t_c)$ have an opposite time dependence; $G_{gr}(t_c)$ shows an exponential decay and $G_{rg}(t_c)$ an exponential growth, because $^{D0}F_1 > {}^{D}F_1$. The validity of eq 14 is based on the condition that the contribution of diffusion to the cross-correlation data (similar to $G_{Diff}(t_c)$ in eq 13) can be neglected. Otherwise, the data analysis would be significantly complicated.

Materials and Methods

Samples. The dyes rhodamine 110 (Rh110, excitation maximum 500 nm, emission maximum 525 nm; Radiant Dyes, Wermelskirchen, Germany), MR121 (excitation maximum 650 nm, emission maximum 665 nm; Roche Diagnostics, Mannheim, Germany), cyanine 5 (Cy5, excitation maximum 650 nm, emission maximum 670 nm; Molecular Probes, Eugene, OR), Alexa660 (excitation maximum 660 nm, emission maximum 685 nm; Molecular Probes), Alexa680 (excitation maximum 680 nm, emission maximum 700 nm; Molecular Probes), Atto655-DNA (5′-d(CGG CCT ATT AGA TAT TTA TTG CTA T(Atto655) TA CCA, free dye: excitation maximum 665 nm, emission maximum 685 nm; Atto-Tec, Siegen, Germany), and Atto647N-DNA (5′-d(TTG ATT CGG TCT ATG CAA AAA AA T(Atto647N) TGC ATA GAG GAT TGC AA, free dye: excitation maximum 645 nm, emission maximum 670 nm; Atto-Tec) were used for control measurements. Stock solutions of these dyes were diluted in double-distilled water to a final concentration of $\approx 10^{-9}$ M for FCS and $\approx 10^{-12}$ M for single-molecule studies.

A double-stranded DNA molecule labeled with Rh110 or Alexa488 (excitation maximum 500 nm, emission maximum 524 nm; Molecular Probes) and Cy5 was applied for FRET measurements, denoted FRET conjugate throughout. The (−)-strand 5′-d(GCA TCG ATC CTC ATT A***T***-A AGT) was labeled with Alexa488 or Rh110 at thymidine residue 17 (bold and italic) using an amino-modified C6 dT from Glenresearch with a donor−acceptor distance of four intervening base pairs. The complementary (+)-strand 3′-d(GCT AGC TAG GAG TAA TAT TCA)−Cy5 was labeled with Cy5 via a C6 aminolinker at its 5′ end. An oligonucleotide of the same sequence without Cy5 was used as a complementary strand for control measurements of FRET-inactive conjugate. The aqueous measurement buffer of the FRET conjugates ($\approx 10^{-12}$ M) contained 180 mM NaCl, 10 mM NaH_2PO_4/Na_2HPO_4, and 400 μM ascorbic acid.

The cross-correlation analysis of Figure 7B was performed with a 62-base-pair DNA strand (Evotec, Hamburg, Germany), which was labeled with rhodamine green (RhGr, excitation maximum 500 nm, emission maximum 525 nm; Molecular Probes) and MR121.

Fluorescence Detection. All experiments were performed with a confocal epi-illuminated fluorescence microscope (IX70 microscope; Olympus, Tokyo, Japan), which has been described previously.[24,29,30] An argon ion laser (Innova Sabre; Coherent, Palo Alto, CA) tuned to 502 or 496 nm was used for excitation of donor fluorescence and FRET either in the continuous wave (cw) or actively mode-locked pulsed mode (APE, Berlin, Germany; pulse length ≈180 ps, repetition rate 73.5 MHz). Either a cw krypton ion laser (Innova 400; Coherent) tuned to 647 nm or a pulsed diode laser at 633 nm (PDL 800; Picoquant, Berlin, Germany; pulse length ≈100 ps, repetition rate synchronized to the actively mode-locked argon ion laser) was employed in the case of direct excitation of fluorescence from the red-emitting or acceptor dye. The laser light was coupled into the microscope by a dichroic mirror (502/636PC; AHF Analysentechnik, Tuebingen, Germany). A water immersion microscope objective (Olympus UplanApo, 60×, N.A. 1.2) was used to focus the laser light into the sample solution and to collect the fluorescence light. The fluorescence light was imaged onto the confocal pinhole and divided into parallel and perpendicular polarized beams and then into two different wavelength ranges below and above 620 nm (dichroic mirror 620DCXR; AHF), and each component was detected by a separate avalanche photodiode (APD-AQR 15; Perkin-Elmer Optoelectronics, Fremont, CA) with separate fluorescence filters (HQ535/50 and HQ730/140; AHF). For each wavelength range (below 620 nm (HQ535/50) denoted green and above 620 nm (HQ730/140) denoted red), the fluorescence photons detected for parallel and perpendicular polarization were combined. Thus, fluorescence is monitored in two detection channels, the green detection channel for the fluorescence of the donor dye (denoted by the index "g") and the red detection channel for the fluorescence of the acceptor dye (denoted by the index "r"). The single-photon detection events were stored by a PC card (SPC 432; Becker & Hickl GmbH Berlin, Germany), which recorded the arrival time since the last photon, the detection channel ("g" or "r"), and in the case of pulsed excitation the microscopic time relative to the next laser pulse for time-correlated single-photon counting (TCSPC) analysis. For single-molecule studies, photons from fluorescence bursts were distinguished from the background signal of 1−2 kHz by applying certain threshold criteria, which have been described in detail before.[21,24,28,67] Correlation data were either software calculated from the photon stream of all selected single-molecule fluorescence bursts or set up by a hardware correlator PC card (5000E, ALV, Langen, Germany) for FCS bulk studies.

All experiments were carried out at room temperature on freely diffusing molecules in an open detection volume. The focal irradiance, I_0, was calculated from the average excitation power, P, and the focal $1/e^2$ radius, ω_0, as determined by FCS of an aqueous Rh110 solution ($D = 3 \times 10^{-6}$ cm^2/s,[68] see eq 12) at low excitation irradiance; $I_0 = P/(\pi/2\omega_0^2)$. The transit time, t_t, of a molecule was calculated from its characteristic diffusion time, τ_{Diff}, determined by FCS; $t_t = 4/3\tau_{Diff}$.[6,15,48,49]

Results and Discussion

Photobleaching of Red-Emitting Dyes by Green Excitation Light. First, we analyzed the influence of simultaneous red and green excitation light on the fluorescence properties of several red-emitting dyes in aqueous solution. Laser wavelengths of 496 or 502 and 647 nm were chosen as green and red excitation light, respectively. We investigated the free dyes Cy5, MR121, Alexa660, and Alexa680 as well as the dyes Atto647N and Atto655 bound to DNA (denoted Atto647N-DNA and Atto655-DNA). It should be noted that fluorescence is solely elicited by the red light. Direct excitation by green light is negligible. Figure 2A shows the abrupt decrease of the fluorescence count rate of

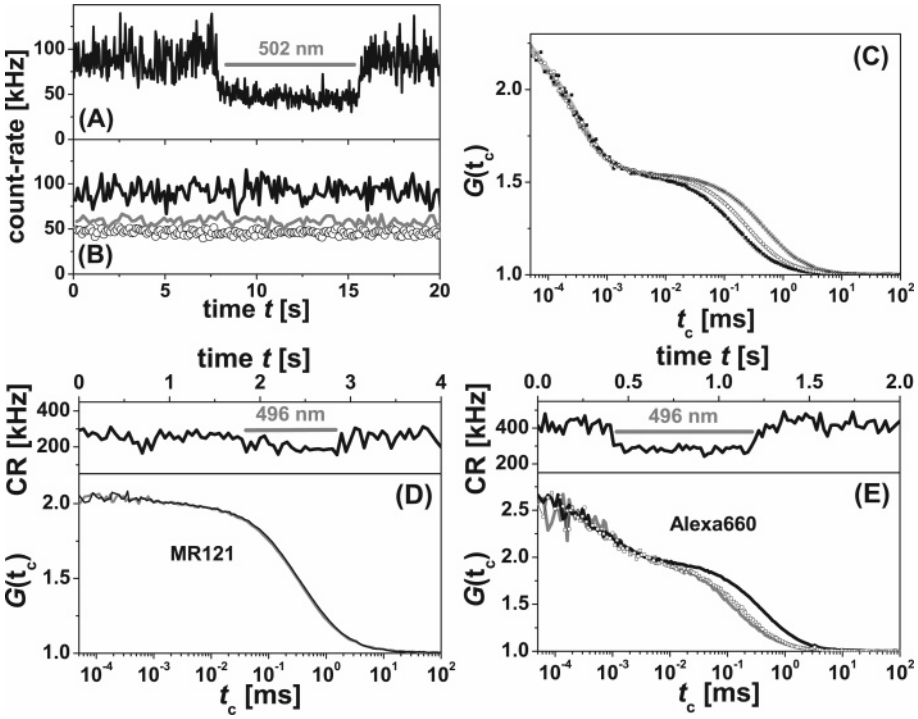

Figure 2. Two-color photobleaching observed by FCS. (A and B) Fluorescence signal of an aqueous Cy5 solution ($\sim 10^{-9}$ M) excited with 647 nm cw laser light ($I_0 = 110$ kW/cm^2) under the addition of 502 nm cw laser light: (A) intermittent addition of 502 nm light ($I_0 = 180$ kW/cm^2); (B) continuous addition of 502 nm with increasing irradiance, $I_0 = 0$ kW/cm^2 (black line), $I_0 = 180$ kW/cm^2 (gray line), and $I_0 = 360$ kW/cm^2 (dots). (C) FCS data resulting from the autocorrelation of the count-rate traces of part B ($I_0 = 0$ kW/cm^2 (crosses), $I_0 = 180$ kW/cm^2 (open dots), and $I_0 = 360$ kW/cm^2 (black squares)). The autocorrelation curves are normalized to the curve at 0 kW/cm^2 irradiance. A fit of eq 13 to these data regarding two dark states (gray lines) results in the following parameters. $I_0 = 0$ kW/cm^2: $c = 1.8$, $\tau_{Diff} = 0.45$ ms, $\omega_z/\omega_0 = 3$, $F_D = 0.24$, and $\tau_{Dark} = 1.0$ μs for the first dark state and $F_D = 0.50$ and $\tau_{Dark} = 0.26$ μs for the second dark state, $A = 0$. $I_0 = 180$ kW/cm^2: $c = 1.7$, $\tau_{Diff} = 0.45$ ms (fixed), $\omega_z/\omega_0 = 3$ (fixed), $F_D = 0.25$, and $\tau_{Dark} = 1.2$ μs for the first dark state and $F_D = 0.53$ and $\tau_{Dark} = 0.23$ μs for the second dark state, $A = 0.55$, $k_z = 2440$ s^{-1}. $I_0 = 360$ kW/cm^2: $c = 2.1$, $\tau_{Diff} = 0.45$ ms (fixed), $\omega_z/\omega_0 = 3$ (fixed), $F_D = 0.24$, and $\tau_{Dark} = 1.3$ μs for the first dark state and $F_D = 0.51$ and $\tau_{Dark} = 0.30$ μs for the second dark state, $A = 0.65$, $k_z = 5000$ s^{-1}. (The experimental conditions were the following: $\omega_0 = 0.7$ μm (τ_{Diff}(Rh110) = 0.4 ms).) (D and E) Two-color photobleaching of MR121 (D) and Alexa660 (E). (upper panel) Fluorescence signal of an aqueous MR121 or Alexa660 solution ($\sim 10^{-9}$ M) excited with 647 nm cw laser light ($I_0 = 170$ kW/cm^2 for MR121 and $I_0 = 70$ kW/cm^2 for Alexa660) under the intermittent addition of 496 nm cw laser light ($I_0 = 250$ kW/cm^2). (lower panel) FCS data resulting from the autocorrelation of the count-rate traces of the aqueous MR121 or Alexa660 solution with simultaneous illumination by 647 nm light ($I_0 = 170$ kW/cm^2 for MR121 and $I_0 = 70$ kW/cm^2 for Alexa660) and 496 nm light ($I_0 = 0$ kW/cm^2 (black line), $I_0 = 140$ kW/cm^2 (open dots), and $I_0 = 250$ kW/cm^2 (gray line)). The autocorrelation curves are normalized to the curve at 0 kW/cm^2 irradiance.

an aqueous Cy5 solution excited by red cw light upon the addition of green cw light. The decrease is enhanced with the green irradiance, as depicted in Figure 2B. This characteristic is common for all other red-emitting dyes investigated here, as exemplarily shown in Figure 2D and E for the free dyes MR121 and Alexa660. To investigate the origin of this fluorescence decrease further, FCS measurements were performed. Figure 2C shows autocorrelation data of Cy5 fluorescence recorded at a constant red irradiance and increasing green irradiance. The decrease in the decay time of the correlation data results from an on average shortened observation time of the Cy5 dye and scales with the green irradiance. This feature of the correlation data is also observed for the other red-emitting dyes (e.g., see Figure 2D and E for MR121 and Alexa660). Due to its dependence on the green irradiance, this effect is assigned to an enhanced photobleaching[48,49,63,69,70] by the green light.

The autocorrelation data of Cy5 (Figure 2C) and of the other red-emitting dyes shows an additional decay in the microsecond time range. The amplitude of this decay differs between the different dyes examined (e.g., compare parts C−E of Figure 2) and rises with the red excitation irradiance. It is assigned to the population of the dye's dark states, which is for the most part the triplet state.[62] Only in the case of Cy5, an additional decay shows up in the sub-microsecond time range. This decay is characteristic for many cyanine dyes, including Cy5, and is caused by photoisomerization kinetics between a dark cis state and a fluorescent trans state.[64,65]

A fit of eq 13 to the FCS data yields values of the equilibrium fraction of the dark state population, F_D, the dark state correlation time, τ_{Dark}, and the effective photobleaching rate constant, k_z, and exposes details of the involved photokinetics, as described next.

(A) Photoisomerization of Cy5 with $F_D \approx 0.5$ and $\tau_{Dark} < 0.5$ μs. Upon excitation, the dye Cy5 shows a fast equilibrium between its cis state and its trans state with about 50% population of the dark cis state. While this population remains constant, the correlation time, τ_{Dark}, decreases with increasing red excitation irradiances. These characteristics of the photo-induced isomerization of Cy5 have in detail been studied before using FCS.[64,65] Most importantly for our experiments, the photoisomerization-characteristic decay in the autocorrelation data does not depend on the green irradiance. Consequently, the green light does not seem to have an influence on the photoisomerization kinetics of Cy5. Thus, within our photokinetic model of the dye Cy5, the photoisomerization can be neglected and treated in terms of a reduced fluorescence quantum yield, Φ(Cy5) $\approx$ 20−30%.

(B) Population of the Triplet State. The rate constants of intersystem crossing (ISC) from S_1 to T_1, k_{ISC}, and of the decay of T_1 to S_0, k_T (see Figure 1A), can be calculated from the

TABLE 1: Results of the Two-Color FCS Measurements; Photokinetic Constants Assigned to the Red-Emitting Dyes

	σ_{01}[a]	τ[b]	k_{ISC}[c]	k_T[c]	σ_{bXn}[d]	σ_{bn}^{eff}[e]
MR121	3.9	1.9	0.09	0.60	0.04	0.06
Cy5	9.6	1.0	1.1	0.50	0.10	0.45
Alexa660	4.4	1.2	5.6	0.57	0.12	1.3
Alexa680	4.3	1.2	3.1	0.30	0.08	0.9
Atto647N-DNA	5.7	4.25	0.12	0.12	0.10	0.21
Atto655-DNA	4.2	2.75	0.21	0.10	0.05	0.17

[a] Absorption cross section at 647 nm, [10^{-16} cm^2]. [b] Average fluorescence lifetimes measured by time-correlated single-photon counting (TCSPC), [10^9 s^{-1}]; especially the decays of the linked dyes are not single exponential. [c] Rate constants of ISC between S_1 and T_1, k_{ISC}, and T_1 and S_0, k_T, determined by FCS corresponding to the method described in the text, [10^6 s^{-1}]. [d] Composite cross section of photobleaching from S_n and T_n for green light (eq 2), [cm^2 W^{-1} s^{-1}]. σ_{bXn} cannot be distinguished between the singlet ($X = S$) and triplet ($X = T$) systems. [e] Effective cross section of higher-order photobleaching for green light (eq 6), [cm^2 W^{-1} s^{-1}].

determined amplitude and correlation time, F_D and τ_{Dark}, of the triplet decay of the FCS data corresponding to $k_{ISC} = F_D/\tau_{Dark}(1 + k_0/k_{01})$ and $k_T = (1 - F_D)/\tau_{Dark}$.[24,62] The inverse fluorescence lifetime of the dyes, k_0, and the rate of excitation, $k_{01} = \sigma_{01}I$ (eq 2), were determined by time-correlated single-photon counting (TCSPC) and calculated from the applied red laser irradiance, I, and the excitation cross section, σ_{01}, at the applied wavelength, respectively. Table 1 lists the resulting values of k_{ISC} and k_T as well as of k_0 and σ_{01} of all dyes examined. The dyes show differences of 1 order of magnitude in their rates of ISC. The values $k_{ISC} \approx 10^6$ s^{-1} and $k_T \approx 10^5$ s^{-1} coincide very well with values previously determined for cyanine or rhodamine dyes via FCS.[62,64] In contrast, the dyes MR121, Atto655, and Atto647N show almost negligible population of the triplet state (e.g., Figure 2D), and corresponding very low values of $k_{ISC} < 2 \times 10^5$ s^{-1}. A slight increase in the triplet lifetime, k_T^{-1}, is observed for the two dyes Atto655-DNA and Atto647-DNA, which are bound to DNA. The triplet state of dyes dissolved in water is to a major extent quenched by water-dissolved oxygen.[47,62] The triplet-quenching efficiency of the oxygen is slightly decreased due to steric hindrance of the DNA.[24] The determined values of k_{ISC} and k_T did not show any dependence on the applied red or green irradiance. Thus, an influence of photoinduced (reverse) ISC can be neglected, at least at the irradiances applied in these measurements (<100 kW/cm^2 for red light and <400 kW/cm^2 for green light). Photoinduced ISC as well as reverse photoinduced ISC specifies the possibility of singlet−triplet crossing via higher excited electronic states.[61,65,71−74] In contrast to our FCS measurements on the free dye Cy5 in solution, photoinduced reverse ISC has been reported for Cy5 attached to a peptide in poly(vinyl alcohol) (PVA)[61] or immobilized on an air−glass interface.[74] It seems that the attachment to the peptide or the PVA or air−glass environment facilitates the photoinduced reverse ISC properties of Cy5.

(C) Photobleaching by Green Light. The values of k_z from the analysis of the FCS data increase with the green excitation irradiance, which follows from the decrease in the decay time of the correlation data. The rate of bleaching should, however, in principle not depend on the green excitation irradiance, since the green light does not directly excite the investigated red-emitting dyes. The addition of green light must open up new bleaching channels, most probably due to excitation from the first to higher excited singlet and triplet states. These states couple quite efficiently with ionic states in polar solvents, such as water, and thus show a large bleaching reactivity.[47−51] These bleaching channels of higher order in irradiance have several times been identified as the major photobleaching pathways in confocal fluorescence microscopy and are already present at cw excitation.[47−49,63,70] This bleaching pathway is quantified by the composite cross section for photobleaching from higher excited states, $\sigma_{bXn} = \sigma_{bSn}$ or σ_{bTn} (eq 2). σ_{bXn} cannot be distinguished between the singlet ($X = S$) and triplet ($X = T$) systems, and its value is thus treated to have the same magnitude, $\sigma_{bSn} = \sigma_{bTn} = \sigma_{bXn}$. Under the experimental conditions used here, with irradiances between 100 and 500 kW/cm^2, direct photobleaching from S_1 and T_1 is much lower than the higher-order photobleaching. As an example, with a typical value of $\sigma_{bXn} = 0.1$ cm^2 W^{-1} s^{-1} (see Table 1), the rate for higher-order photobleaching at an excitation irradiance of $I \approx 100$ kW/cm^2 amounts to $k_{bXn} = \sigma_{bXn}I \approx 10\,000$ s^{-1}, which is 1−2 orders of magnitudes larger than values of the rate constant, $k_{b1}^{eff} = 100-1000$ s^{-1}, known for photobleaching from S_1 and T_1.[47] k_{b1}^{eff} is thus neglected, and the values of σ_{bXn} can be directly calculated by eq 6 using the previously determined photophysical parameters listed in Table 1 and the values of k_z determined from the FCS data.

All investigated dyes show a significant amount of higher-order photobleaching upon the addition of green light. The cross sections, σ_{bXn}, lie in a range of 0.03−0.1 cm^2 W^{-1} s^{-1}, which is 2 orders of magnitude larger than values of $\sigma_{bXn} \approx 0.001-0.005$ cm^2 W^{-1} s^{-1}, previously obtained for direct two-step photolysis of free rhodamine 6G at 502−532 nm laser excitation.[48,49] These enhanced values can be caused by several effects: (1) Generally, red-emitting dyes have lower ionization potentials, leading to a higher bleaching reactivity from the higher electronic states. (2) The absorption cross section to higher excited electronic states might be more pronounced at around 500 nm. (3) The higher energy of a green photon compared to a red one leads to a higher level of excitation of S_n and T_n, closer to the ionization level and, thereby, to an increased bleaching reactivity. Note, that we have not observed any higher-order photobleaching due to the red excitation light, at least not at the applied irradiances <100 kW/cm^2.

Due to its relatively long lifetime (microseconds compared to nanoseconds for the singlet state), the triplet state has in a lot of cases been identified as the major pathway of (higher-order) photobleaching.[47−49] A real comparison of the extent of higher-order photobleaching between the different dyes therefore has to include the triplet population, as done by the effective cross section, σ_{bn}^{eff} (eq 6). The previously determined composite cross section for photobleaching from higher excited states, $\sigma_{bXn} = \sigma_{bSn}$ or σ_{bTn} (eq 2), solely quantifies the efficiency of higher-order photobleaching starting from S_1 or T_1. In contrast, σ_{bn}^{eff} represents the overall efficiency of higher-order photobleaching after the incident of excitation to S_1. The values of σ_{bn}^{eff} can be calculated from σ_{bXn} applying the determined triplet parameters, k_{ISC} and k_T (eq 6 and Table 1). While the values of σ_{bXn} are about in the same range for the different dyes, the values of the effective cross section, σ_{bn}^{eff}, differ by an order of magnitude (Table 1). σ_{bn}^{eff}, and thus photobleaching in general, is extremely low for those dyes that show a very low rate of intersystem crossing, that is, MR121, Atto647N, and Atto655. As an example, the low photobleaching reactivity of MR121 becomes obvious from the almost diminishing decrease in count rate or FCS decay time upon the addition of green light (see, e.g., Figure 2D). This characteristic emphasizes the important role of the triplet state in the photostability of dyes.

The observed results show the tremendous impact of green laser light on the photoreactivity of the red-emitting dyes. The amount of green light should therefore carefully be chosen in

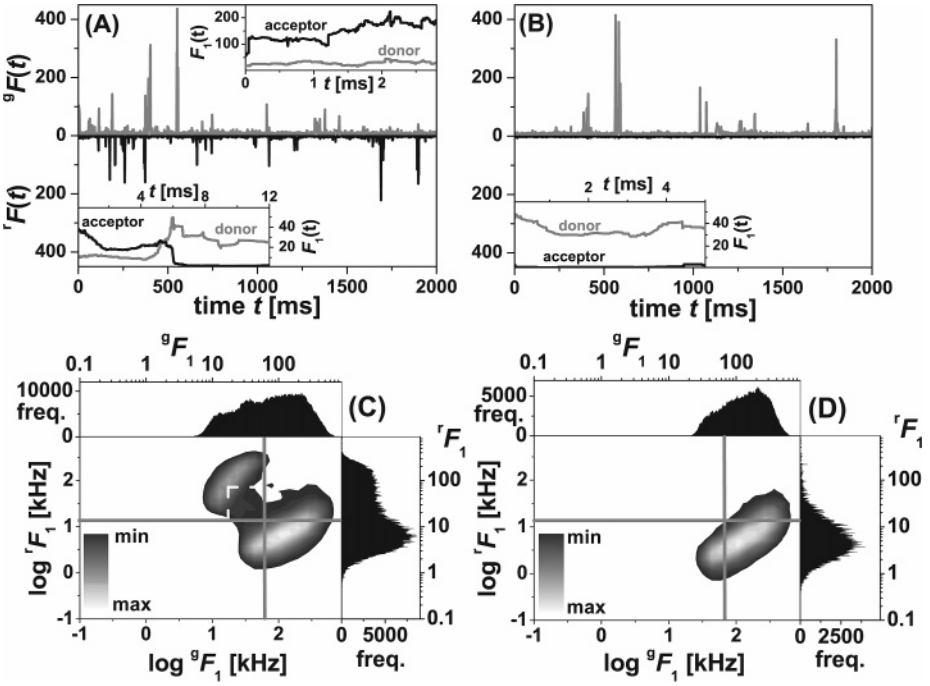

Figure 3. Single-molecule FRET analysis. Fluorescence count rate, ${}^{g}F(t)$ and ${}^{r}F(t)$ (time resolution 1 ms), recorded in the donor detection channel (upper panel) and in the acceptor detection channel (lower panel) for single FRET conjugates labeled with Alexa488 and Cy5 (A) and solely labeled with Alexa488 (B). The insets of parts A and B show exemplary time trajectories of the fluorescence brightness, $F_1(t)$, determined from consecutive bins of 100 photons within a single fluorescence burst for the donor and acceptor detection channels. (C and D) Two-dimensional parameter histograms of fluorescence brightness pairs simultaneously detected for the donor, ${}^{g}F_1$, and acceptor, ${}^{r}F_1$, together with one-dimensional projections (freq. = frequency). The histograms were set up from the time trajectories, $F_1(t)$, of several single-molecule fluorescence bursts for the FRET conjugate labeled with Alexa488 and Cy5 (5392 single-molecule events) (C) and solely labeled with Alexa488 (2656 single-molecule events) (D). The gray lines in parts C and D mark the selection criteria for distinguishing between fluorescence bursts from the FRET-active (upper left quadrant) and FRET-inactive (lower right quadrant) subpopulations. The area marked by the dashed gray line in part C reveals intermediate brightness values. (The experimental conditions were the following: pulsed excitation at 502 nm, $I_0 = 95$ kW/cm^2, $\omega_0 = 0.6$ μm (τ_{Diff}(Rh110) = 0.3 ms).)

two-color fluorescence experiments combining simultaneous green and red laser excitation, and in particular at or close to saturation. The choice of irradiance is of particular importance in FRET experiments, where the excited acceptor dye is intrinsically exposed to green light, as characterized in the next chapter.

Acceptor Photobleaching in FRET Experiments

Single-Molecule Analysis. Single-molecule experiments of the FRET conjugate were performed at different irradiances of 502 nm in order to characterize the impact of the green laser light on the acceptor photoreactivity in FRET experiments. Figure 3 shows a typical single-molecule experiment of FRET-active (Figure 3A) and FRET-inactive (Figure 3B) conjugates (in this case applying Alexa488 and Cy5 labels), clearly presenting fluorescence bursts above the background signal level due to single-molecule transits. By selecting only photons within a fluorescence burst, that is, from a single-molecule transit, for subsequent analysis, time trajectories of the donor and acceptor brightness, $F_1(t)$, were set up for each single-molecule event from a so-called sliding-photon window analysis.[21,24,28,29,67] Here, the photon stream detected within a single-molecule event was split up into subsequent windows of 100 photons each. For each photon window, the brightness was calculated from the corresponding length of time ($F_1 = 100$/length of time) and the point in time, t, taken from the 50th photon event. The insets to Figure 3A and B show examples of such time trajectories, $F_1(t)$. In particular, the inset of the lower panel of Figure 3A depicts an event of acceptor photobleaching, characterized by an abrupt loss in acceptor brightness and an accompanying increase in donor brightness due to the breakdown of FRET (see Figure 1B).

It is surprising that the height of the fluorescence bursts in the donor detection channel is the same for donor- and acceptor-labeled conjugates and for solely donor-labeled conjugates (Figure 3A and B). The presence of fluorescence bursts in the acceptor channel reveals the FRET activity in the case of doubly labeled conjugates, which should lead to a decrease in the fluorescence brightness of the donor. For a better understanding, two-dimensional joint histograms of coincident donor and acceptor brightness were set up from the single-molecule trajectories, $F_1(t)$ (Figure 3C and D). Such an analysis method has been introduced previously and enables the exposure of species of one sample with different FRET activities.[24,27,29−31] Two species are exposed in this case, that is, a FRET-active species with high brightness, ${}^{r}F_1$, in the acceptor detection channel and low brightness, ${}^{g}F_1$, in the donor detection channel and a FRET-inactive species with hardly any brightness in the acceptor detection channel and high brightness, ${}^{g}F_1$, in the donor detection channel. Thus, FRET activity is accompanied by high fluorescence bursts in the acceptor detection channel and simultaneously low bursts in the donor detection channel. For the case of FRET inactivity, this is vice versa. Intermediate cases (dashed gray line in Figure 3C) are caused by fast acceptor bleaching or by very rare events of multiple molecules simultaneously traversing the detection volume. Recent work reports photodestruction-intermediate states of an acceptor dye that are nonemitting but still able to quench the fluorescence of the donor.[57] Such a molecule is characterized by a quenched, low donor and no acceptor fluorescence. However, such

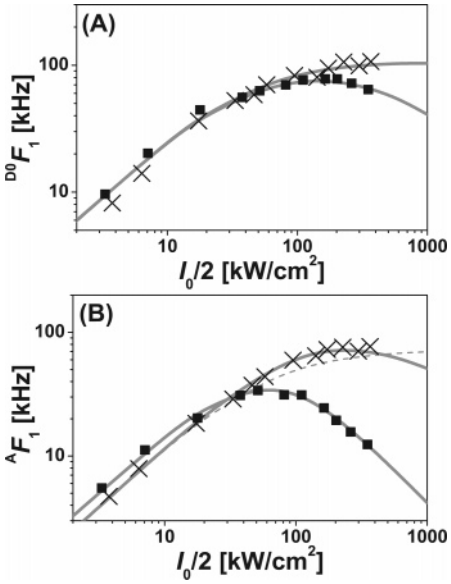

Figure 4. Irradiance dependence of donor and acceptor brightness. Dependence of the average brightness, F_1, of single Rh110- and Cy5-labeled FRET conjugates on the irradiance, $I_0/2$, of cw (crosses) and pulsed (black squares) 502 nm laser light: donor, $^{D0}F_1$ (A), and acceptor, $^{A}F_1$ (B), fluorescence. The brightness in part A was determined from FRET-inactive fluorescence bursts, and that in part B was determined from FRET-active fluorescence bursts, selected as outlined in Figure 3C. All data could be well described by eq 11 utilizing eq 4 in the case of pulsed excitation and eq 7 in the case of cw excitation as well as the corresponding photokinetic constants listed in Table 2 (gray lines). The dashed gray line represents the simulation disregarding photoinduced (reverse) intersystem crossing and photobleaching. (The experimental conditions were the following: $\tau_{Diff} = 1$ ms, $\omega_0 = 0.6$ μm (τ_{Diff}(Rh110) = 0.3 ms).)

photodestruction-intermediate states have not been observed in any of the single-molecule trajectories.

As outlined, the FRET-inactive species is to a substantial portion also present in the case of the single-molecule studies of the donor- and acceptor-labeled conjugate. As shown in a previous study,[43] this portion appears despite intact double labeling due to inactive or missing acceptor dye. Insufficient hybridization of the double DNA strand can be excluded for at least two reasons. First, potential residual single-stranded DNA was removed during the synthesis of the conjugates. Second, the breakup of the FRET-active double strand into two inactive single strands after the dilution to the picomolar concentration should lead to a rise of the fraction of FRET-inactive conjugates over time. No such time dependence could be observed.

The gray lines in Figure 3C and D mark the selection criteria for distinguishing between fluorescence bursts from FRET-active molecules (upper left quadrant) and FRET-inactive molecules (lower right quadrant). By selecting only photon bursts from the FRET-active species, the analysis is solely focused on the truly FRET-active molecules. This artifact-free analysis can only be achieved by single-molecule analysis, a reason for our choice of analysis method in this case.

Irradiance Dependence of Fluorescence Brightness. Figure 4 shows the dependence of the average brightness, F_1 (number of counts per dwell time), per single-molecule burst on the excitation irradiance of green light at 502 nm, for the donor of the FRET-inactive species and for the acceptor of the FRET-active species, in this case of a Rh110- and Cy5-labeled FRET conjugate. The donor and acceptor brightness coincides with the brightness detected in the corresponding detection channels, $^{D0}F_1 = {}^{g}F_1$ and $^{A}F_1 = {}^{r}F_1$ (eq 11). Cross-talk of donor fluorescence into the acceptor detection channel, α (eq 11), makes up less than 2% and can be disregarded for the FRET-active species (see Figure 3C). Using cw (crosses) or pulsed (squares) excitation, the irradiance dependence of F_1 shows three typical regimes, as was also observed in previous studies:[47−49,70] (1) a linear dependence for low irradiance, (2) a saturation to a maximum value due to triplet or dark state population and photobleaching, and (3) a pronounced decrease for high irradiances, which can only be explained by a high degree of photobleaching reactivity from higher excited electronic states. This decrease is exceptionally pronounced for the acceptor fluorescence brightness in the case of pulsed excitation. All of the data can be well described by eq 11 (utilizing eq 4 for pulsed excitation and eq 7 for cw excitation). This description (gray lines) uses the photophysical constants of Table 2 and introduces products of fluorescence detection efficiency and fluorescence quantum yield of $\Psi_g\Phi_{D0} = 0.0055$ for the donor and $\Psi_r\Phi_A = 0.0027$ for the acceptor in the case of cw excitation and 0.0033 in the case of pulsed excitation. Detection efficiencies in the range of $\Psi \approx 1-5\%$ generate reasonable values for the quantum yields of donor, $\Phi_{D0} \approx 0.1-0.6$, and acceptor, $\Phi_A \approx 0.05-0.30$, which might be slightly lower compared to the free dye due to dark states involved when coupled to the DNA.[67]

(A) Irradiance Dependence of the Donor. A slight difference is observed between pulsed (squares) and cw (crosses) excitation for the irradiance dependence of the fluorescence brightness, $^{D0}F_1$, of the donor of the FRET-inactive species (Figure 4A). On one hand, the maximum achievable photon counts are slightly lower for the case of pulsed excitation. This is caused by pulse saturation, which has in detail been outlined in previous publications.[49,69,75] Compared to cw excitation, the increased peak irradiance of the picosecond pulses leads to a pronounced degree of saturation of the optical S_0-S_1 transition, resulting in about a 1.5-times higher achievable brightness for cw excitation. This finding is in accordance with the factor of about 1.4 resulting from our experiments. Most prominent, however, is photobleaching from higher excited electronic states manifested in a more pronounced decrease of the brightness toward very high irradiances observed for pulsed excitation. The composite cross section, $^{D0}\sigma_{bXn}$ (eq 2), for photobleaching from higher excited electronic states is 1 order of magnitude higher for pulsed excitation (0.0016 cm^2 W^{-1} s^{-1}) than for cw excitation (0.0001 cm^2 W^{-1} s^{-1}) (Table 2). Pulse enhancement of higher-order photobleaching may in general be explained by the amplification of multistep excitation due to the significantly enhanced photon density condensed within the pulses.[49]

While the absolute values of $^{D0}\sigma_{bXn}$ lie within values of $\sigma_{bXn} \approx 0.001-0.005$ cm^2 W^{-1} s^{-1}, previously reported for direct two-step photolysis of other free rhodamine dyes in aqueous solution at 502−532 nm laser excitation,[48,49] it is surprising to note that the same reports do not observe any difference between cw and picosecond pulsed excitation. Coupling of the rhodamine dye to the DNA may result in different photochemical properties such as trapping of photoelectrons.

(B) Irradiance Dependence of the Acceptor. Several other photophysical processes have to be regarded in the case of the FRET-induced acceptor fluorescence. First of all, FRET to the excited singlet and triplet states has to be included besides the energy transfer to the acceptor's ground state (eq 8). If one only considers FRET to the acceptor's ground state (eq 8i), the pronounced excitation of the acceptor at very high irradiances will lead to a depletion of its ground state ($^{A}S_0 \ll 1$). This ground state depletion will result in a decrease of the extent of FRET, which is accompanied by a rise of the donor's lifetime (see eq

TABLE 2: Results of the FRET Photobleaching Measurements; Photokinetic Constants Assigned to the Dyes Rh110 and Cy5 in the FRET Conjugate

	σ_{01}, E^a	τ^b	$k_{ISC}/k_T{}^c$	$k_{bX1}{}^d$	$\sigma_{(Re)ISC\text{-}n}{}^{e,i}$	$\sigma_{bXn}{}^{f,i}$	$\phi^*_{(Re)ISC\text{-}n}{}^{g,i}$	$\phi^*_{bXn}{}^{h,i}$
Rh110	2.36	4.0[j] 0.33[k]	1.1/0.1	13	0	0.0001[l] 0.0016[m]		
Cy5	0.92	1.5	1.1/0.1	350	1.0	0.005[l] 0.025[m]	0.005	2.5

[a] Absorption cross section at 502 nm, [10^{-16} cm^2]. Cy5 is excited via FRET; thus, the energy transfer efficiency, E, is given. [b] Fluorescence lifetime measured by TCSPC, [10^9 s^{-1}]. [c] Rate constants of ISC between S_1 and T_1, k_{ISC}, and T_1 and S_0, k_T, determined by FCS corresponding to the method described in conjunction with Table 1, [10^6 s^{-1}]. [d] Rate constant for direct photobleaching from S_1 and T_1, [s^{-1}]; taken from the literature.[47] [e] Composite cross section of (reverse) ISC from S_n and T_n for green light (eq 2), [cm^2 W^{-1} s^{-1}]. [f] Composite cross section of photobleaching from S_n and T_n for green light (eq 2), [cm^2 W^{-1} s^{-1}]. [g] Quantum yield of (reverse) ISC from S_n and T_n for FRET-induced excitation (eq 10c and d). [h] Quantum yield of photobleaching from S_n and T_n for FRET-induced excitation (eq 10e), [10^{-5}]. [i] These parameters cannot be distinguished between the singlet ($X = S$ or ISC) and triplet ($X = T$ or ReISC) systems. [j] FRET-inactive conjugate. [k] FRET-active conjugate. [l] cw excitation. [m] Pulsed excitation.

10a). However, this is not observed here; a constant donor lifetime of $\tau_D = 0.33$ ns is measured over the whole range of excitation irradiance for the FRET-active species. With $\tau_{D0} = 4$ ns in the absence of FRET to an acceptor, one can estimate the energy transfer efficiencies to $E_{S0} = E_{S1} = E_{T1} = 0.92$ (eq 10a). Additional energy transfer pathways of this type have previously been reported for single bichromophoric dye systems[60] and have in particular for Cy5 been observed to be as effective as FRET to the singlet ground state.[61]

Surprisingly, the experimentally determined brightness of the acceptor is underestimated and its power dependence cannot be described properly if we disregard any photobleaching and assume the energy transfer efficiencies of 0.92 and values of σ_{01}, τ, k_{ISC}, and k_T as listed in Table 2 (dashed gray line in Figure 4B for the case of cw excitation). Our simulation may underestimate the fluorescence brightness values for several reasons: (1) Significant direct excitation of Cy5 by the green light may enhance the fluorescence emission but is negligible (<1% of the signal, i.e., ${}^A\sigma_{01} = 0$ in eq 10b) and can be excluded. (2) Photobleaching will result in even lower brightness values at the saturation level. (3) Photoinduced reverse ISC is a very likely mechanism that leads to an increase in fluorescence at higher excitation irradiances, since it recovers dye molecules which have been trapped in the long-living triplet state.[71] This pathway is known for cyanine dyes[65] and particularly for Cy5.[61,74] Thus, to fit the data, (reverse) photoinduced ISC must be included with effective cross sections, ${}^A\sigma_{ISC\text{-}n} = {}^A\sigma_{ReISC\text{-}n} = 1$ cm^2 W^{-1} s^{-1} (eq 2), for the green light and quantum yields, ${}^A\phi^*_{ISC\text{-}n} = {}^A\phi^*_{ReISC\text{-}n} = 0.005$ (eq 10c and d), for FRET to the excited singlet and triplet states (see Table 2). This result is contrary to our FCS experiments (Figure 2), where no (reverse) photoinduced ISC has been observed for free Cy5 in solution. As for previous studies,[61,74] it seems that the attachment of the dye to the DNA or biomolecules in general might introduce this pronounced ISC via the higher excited electronic states.

We cannot distinguish between the singlet and triplet systems from our data and thus cannot determine the exact real values of the corresponding photokinetic parameters. Nevertheless, it is useful to apply the same set of parameter values for the FRET efficiencies to S_1 and T_1 and for photobleaching and photoinduced (reverse) intersystem crossing via S_n and T_n, to prove the existence of such processes. Moreover, the obtained values of ${}^A\sigma_{ReISC\text{-}n} = 1$ cm^2 W^{-1} s^{-1} and ${}^A\phi^*_{ReISC\text{-}n} = 0.005$ coincide very well with values of photoinduced reverse intersystem crossing previously reported for another cyanine dye.[65]

For high irradiances, a significant difference in acceptor brightness is observed between cw (crosses) and pulsed (squares) excitation (Figure 4B). Pulse saturation cannot explain the observed decrease in brightness. Thus, photolysis from higher electronic states needs to be considered. Different values of cross sections, ${}^A\sigma_{bXn}$ (eq 2), and corresponding quantum yields, ${}^A\phi^*_{bXn}$ (eq 10e), for photobleaching via S_n and T_n, by excitation at 502 nm and by FRET had to be employed for a correct description of the irradiance dependence of the brightness; ${}^A\sigma_{bXn} \approx 0.005$ cm^2 W^{-1} s^{-1} and ${}^A\phi^*_{bXn} = 2.5 \times 10^{-5}$ for the acceptor with green cw excitation, and ${}^A\sigma_{bXn} \approx 0.025$ cm^2 W^{-1} s^{-1} and ${}^A\phi^*_{bXn} = 2.5 \times 10^{-5}$ for the acceptor with green pulsed excitation. As in the case of the donor dye, the effective higher-order photobleaching cross section, ${}^A\sigma_{bXn}$, is 5 times larger in the case of pulsed excitation. In both cases, cw and pulsed excitation, photobleaching of the donor has been included by the corresponding values of ${}^D\sigma_{bXn} = {}^{D0}\sigma_{bXn}$ determined for the donor in the absence of FRET. However, its influence is negligible.

Cross-correlation analysis of the single-molecule time trajectories of the FRET-active conjugate was performed to further prove the high degree of photobleaching from higher excited states, evoked by the green excitation light.

Cross-Correlation Analysis of Single-Molecule Time Trajectories. Figure 5A and B presents the cross-correlation curves, $G_{gr}(t_c)$ and $G_{rg}(t_c)$ (eq 14), obtained from the analysis of several single-molecule trajectories of FRET-active species, which have been selected from bursts of the experiments with pulsed excitation. For high irradiances, the data can be well described by eq 15, regarding the population of dark states and acceptor photobleaching. Since the exact theory for photobleaching analysis of FCS experiments with pulsed excitation is very complex, it is for this work sufficient to describe the cross-correlation data by the steady state theory assuming quasi-continuous excitation (eqs 6 and 7). This approximation is possible because the pulse saturation of the acceptor fluorescence is negligible, as mentioned in the case of the data of Figure 4B.[49]

The cross-correlation curves show the behavior predicted from theory (eq 15), an exponential decay in the case of $G_{gr}(t_c)$ and an exponential growth in the case of $G_{rg}(t_c)$. A fit of eq 15 to the cross-correlation data results in values of the effective acceptor photobleaching rate constant, ${}^Ak_z$. As shown in Figure 5C (black squares and crosses), ${}^Ak_z$ increases with irradiance, which is manifested in a shortened decay or rise time of the cross-correlation data. At high irradiances, the data of ${}^Ak_z$ (black squares) can be described by eq 6 applying values listed in Table 2 (gray line). However, this analysis is biased for irradiances of $I_0 < 160$ kW/cm^2 (crosses), as can be observed by the change in the decay characteristics of $G_{rg}(t_c)$ from an exponential growth to an exponential decay (Figure 5B). For these irradiances, the cross-correlation data are substantially hampered by diffusion, since the average time before bleaching, $t_z = 1/{}^Ak_z$, is no longer much shorter than the average transit time, t_t, through the

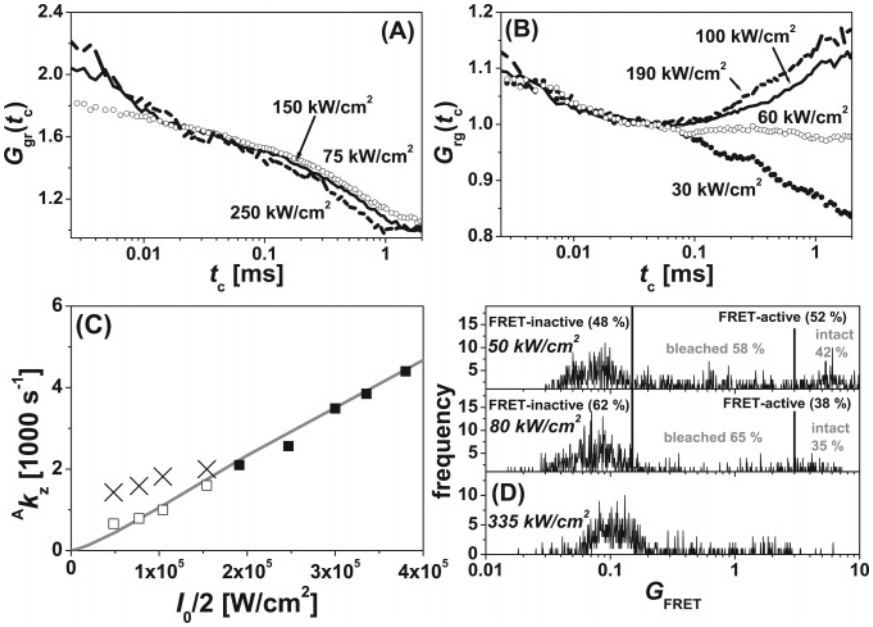

Figure 5. Acceptor photobleaching revealed by single-molecule cross-correlation analysis. Single-molecule analysis of acceptor photobleaching for the FRET-active subpopulation of Rh110- and Cy5-labeled FRET conjugates in the case of pulsed 502 nm excitation. (A and B) Cross-correlation curves, $G_{gr}(t_c)$ and $G_{rg}(t_c)$, obtained from the analysis of fluorescence brightness time trajectories, $F_1(t)$, of several single-molecule fluorescence bursts (between 700 and 2400 depending on the applied irradiance) for different irradiances, $I_0/2$. (C) Values of the effective photobleaching rate constant, ^Ak_z, of the acceptor obtained from a fit of eq 15 to the cross-correlation data of parts A and B (black squares for $I_0/2 > 160$ kW/cm^2 and crosses for $I_0/2 < 160$ kW/cm^2) and from the determination of p_{intact} (eq 6) of part D (open squares). (D) Ratio $G_{FRET} = {}^rF_1/{}^gF_1$ of the fluorescence brightness simultaneously detected in the acceptor and donor detection channels calculated for all single-molecule events of the FRET conjugate for different irradiances, $I_0/2$. The lines at $G_{FRET} = 0.15$ and $G_{FRET} = 3$ mark the threshold criteria for the distinction of FRET-inactive species ($G_{FRET} < 0.15$) and FRET-active species ($G_{FRET} > 0.15$), as well as FRET-active species with and without the incident of acceptor photobleaching ($0.15 < G_{FRET} < 3$ "bleached" and $G_{FRET} > 3$ "intact"). The percentages give the respective fraction of molecules. The probability p_{intact} (eq 6) equals the fraction of intact FRET-active molecules relative to all FRET-active molecules (42% in the upper panel and 35% in the middle panel). Values of p_{intact} cannot reliably be determined at high irradiances (lower panel). The thresholds in G_{FRET} were set in a way to match values in ^Ak_z determined by the cross-correlation analysis. (The experimental conditions were the same as those in Figure 4.)

detection volume. Thus, a correct analysis of these curves has to take acceptor photobleaching linked to diffusion into account, but this did not yield any reliable results. Therefore, another analysis method was applied for low irradiances (open squares).

Counting Specific Single-Molecule Bursts: G_{FRET} Analysis. At low irradiances, the acceptor does not bleach during each single-molecule transit. In this case, it is feasible to count single-molecule bursts which are characterized by a sufficiently high ratio of $G_{FRET} = {}^rF_1/{}^gF_1$ of the fluorescence brightness simultaneously detected in the acceptor and donor detection channels. Analyzing all single-molecule events of the FRET conjugate for different irradiances, Figure 5D depicts the frequency of the bursts for certain values of G_{FRET}. As in Figure 3C, two species are detectable: a FRET-inactive species for $G_{FRET} < 0.15$ and a FRET-active species for $G_{FRET} > 0.15$. By setting a threshold at $G_{FRET} = 3$, we can distinguish between FRET-active molecules just undergoing acceptor photobleaching during the transit ($0.15 < G_{FRET} < 3$) and FRET-active molecules without acceptor photobleaching ($G_{FRET} > 3$). High values of G_{FRET} result from an on average high value of acceptor brightness, indicating no or at least very little acceptor photobleaching.

The fraction of stable molecules ($G_{FRET} > 3$) establishes the survival probability, p_{intact} (eq 6), of still being fluorescent after the transit time, t_t. A reliable determination of p_{intact}, however, is only possible for $I_0/2 < 160$ kW/cm^2, permitting the complementary determination of ^Ak_z to the cross-correlation analysis (open squares in Figure 5C). At higher irradiances, bleaching occurs too early during the transit (lower panel of Figure 5D), resulting in a very low number of intact molecules ($G_{FRET} > 3$). In this case, p_{intact} cannot be calculated accurately.

The theoretical description of the irradiance dependence of ^Ak_z (eq 6) in Figure 5C obtained from the complementary cross-correlation (black squares) and G_{FRET} analysis (open squares) employs the same photophysical model and constants as before (Table 2) and has to include photobleaching from higher excited singlet and triplet states of the acceptor with a cross section of $^A\sigma_{bXn} = 0.033$ cm^2 W^{-1} s^{-1}. This value coincides well with the value 0.025 cm^2 W^{-1} s^{-1} following the analysis of the irradiance dependence of the acceptor's fluorescence brightness of Figure 4D.

Conclusion of the Single-Molecule Acceptor Photobleaching Experiments. The consistent results obtained from the different analysis methods demonstrate that both the maximum accessible fluorescence emission and the observation time in FRET experiments are restricted by photobleaching from higher excited states. The cross sections, $^A\sigma_{bXn}$ (eq 2), for photobleaching from these electronic states of the acceptor are more than 1 order of magnitude larger than the corresponding cross sections of the donor or of rhodamine dyes in general[48,49] and correspond very well with the values of σ_{bXn} deduced from the two-color FCS measurements (see Table 1). Assuming an absorption cross section of $^A\sigma_{T1n} \approx 10^{-16}$ cm^2 (eq 1) for, for example, the triplet state, as previously reported for Cy5,[61] the quantum yield of photobleaching yields $^A\phi_{bXn} \approx 2.5 \times 10^{-5}$ for cw excitation and $^A\phi_{bXn} \approx 1.3 \times 10^{-4}$ for pulsed excitation (see eq 2). While the value of this quantum yield for cw excitation has about the same magnitude as that following FRET, $^A\phi^*_{bXn}$, or that of rhodamine dyes,[48,49] the photobleaching reactivity is enhanced by a factor of 5 in the case of picosecond pulsed excitation. As for the mere photobleaching of the donor, this pulse enhance-

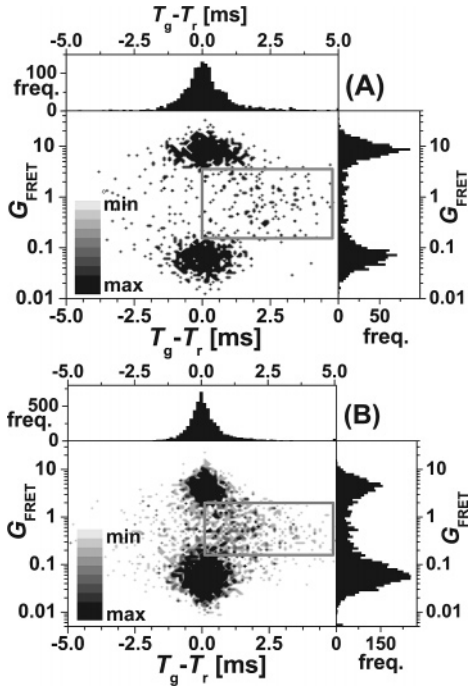

Figure 6. $T_g - T_r$ analysis of the Alexa488- and Cy5-labeled FRET conjugate excited by pulsed laser light at 496 nm with an irradiance of $I_0 = 55$ kW/cm^2 (A) and $I_0 = 110$ kW/cm^2 (B); joint two-dimensional parameter histogram and the respective one-dimensional projections of the time difference $T_g - T_r$ and the ratio $G_{FRET} = {}^rF_1/{}^gF_1$ determined from several single-molecule bursts (1559 in part A and 5630 in part B). T_g and T_r represent the average values of the macroscopic times of all photons detected within a fluorescence burst for the donor and acceptor detection channels, respectively. The macroscopic time depicts the time of the detection of a photon with respect to the beginning of the fluorescence burst (see Figure 1B). The gray box selects single-molecule events with pairs of values ($T_g - T_r$, G_{FRET}) exhibiting acceptor photobleaching (153, i.e., 10%, in part A and 957, i.e., 17%, in part B). (The experimental conditions were the following: $\omega_0 = 0.55$ μm (τ_{Diff}(Rh110) = 0.25 ms).)

ment of higher-order photobleaching may in general be explained by the amplification of multistep excitation due to the significantly enhanced photon density condensed within the pulses. It is surprising that picosecond-long pulses already cause such a gain in photobleaching, since previous studies revealed such pronounced pulse effects only for femtosecond-long pulses.[49] In addition to a slight decline in the maximal achievable fluorescence brightness due to pulse saturation, this strong pulse enhancement of photobleaching hampers the use of (even picosecond) pulsed excitation light to FRET experiments.

Exposure of Significant Acceptor Photobleaching in Single-Molecule Experiments: $T_g - T_r$ Analysis

The $T_g - T_r$ analysis is an easily conceivable method for analyzing the amount of acceptor photobleaching in single-molecule FRET or two-color experiments in general. The present setup permits the tagging of each fluorescence photon event of a single-molecule transit with its macroscopic time relative to the beginning of the transit, as exploited to build up the single-molecule time trajectories of Figure 3. The average value of the macroscopic time tags of all photons detected within a fluorescence burst for the donor and acceptor detection channels, T_g and T_r, respectively, gives the center of the observation time of donor and acceptor fluorescence (Figure 1B).

Figure 6 depicts two-dimensional joint histograms of pairs of values of the ratio $G_{FRET} = {}^rF_1/{}^gF_1$ of the fluorescence brightness simultaneously detected in the acceptor and donor detection channels and $T_g - T_r$ obtained from single-molecule transits of the FRET conjugate (in this case Alexa488- and Cy5-labeled) for two different irradiances. Four features are visible.

(1) FRET-active and -inactive species are distinguishable by their value of G_{FRET} (as has been outlined in Figure 5D). FRET activity results in high fluorescence brightness, ${}^rF_1 = {}^AF_1$, of the acceptor and thus high values of G_{FRET}, while FRET inactivity shows no acceptor emission, ${}^rF_1 \approx 0$, leading to low values of G_{FRET}. Without the incident of acceptor photobleaching, both, acceptor and donor, give rise to a homogeneous fluorescence emission in time throughout the transit and thus to about the same values in T_g and T_r, that is, $T_g - T_r \approx 0$. Even for the case of FRET inactivity, the signal in the acceptor channel due to cross-talk or background signal should be distributed homogeneously in time within the burst.

(2) Very rare events of the transit of several molecules within one fluorescence burst (accidental multimolecule events) expose intermediate values of G_{FRET} and larger values of $T_g - T_r$ that are symmetrically distributed around zero, because multimolecule events might be due to the simultaneous transit of, for example, FRET-active and -inactive species.

(3) Single-molecule events expressing intermediate values of G_{FRET} and positive, asymmetric distributed values of $T_g - T_r > 0$ are characteristic for acceptor photobleaching (gray box in Figure 6). Intermediate values of G_{FRET} have already been utilized for the calculation of p_{intact} in Figure 5D. On the other hand, the photobleaching of the acceptor dye shortens the time period of its fluorescence emission and leads to a simultaneous rise in the fluorescence photon emission of the donor. As sketched in Figure 1B, such an event leads to higher values in T_g and shortened times T_r. Thus, a positive value of the difference $T_g - T_r > 0$ readily expresses the event of acceptor photobleaching. The amount of single-molecule events within this (G_{FRET}, $T_g - T_r$) sector (gray lines) scales with the applied irradiance and quantifies the extent of acceptor photobleaching (10% in Figure 6A and 17% in Figure 6B).

(4) Excessive photobleaching of the acceptor furthermore results in a lower brightness of the acceptor, ${}^rF_1 = {}^AF_1$ (see Figure 4), and thus, $G_{FRET} = {}^rF_1/{}^gF_1$, as can be observed from the comparison of parts A and B of Figure 6.

In this case, we have constituted a slightly modified FRET conjugate with the dye Alexa488 as the donor and pulsed excitation at 496 nm to exemplify that extensive acceptor photobleaching is not a problem specific to the previously applied FRET conjugate at 502 nm laser excitation.

The $T_g - T_r$ analysis thus enables the optimization of experimental conditions with respect to photobleaching. The increased amounts of events in the marked (G_{FRET}, $T_g - T_r$) sector (gray box in Figure 6) reveal a significant increment in acceptor photobleaching at higher irradiances. In addition to the adjustment of the irradiance, the exposed excess of photobleaching can be minimized by the addition of certain chemicals such as ascorbic acid. The favorable stabilization effect of ascorbic acid is well-known, especially for the case of photolysis from higher excited electronic states involving ionic states,[47,70,76] a reason for the addition of ascorbic acid to the buffered solution of FRET conjugate from the initial stages of our experiments.

We have to note that the $T_g - T_r$ analysis is not confined to FRET experiments but enables one to readily check the amount of photobleaching of any of the involved dyes in multicolor experiments. More generally speaking, this method can directly characterize the coincidence of the fluorescence signal in multicolor experiments and thus directly expose the existence of multiple species or conformational states of a sample.

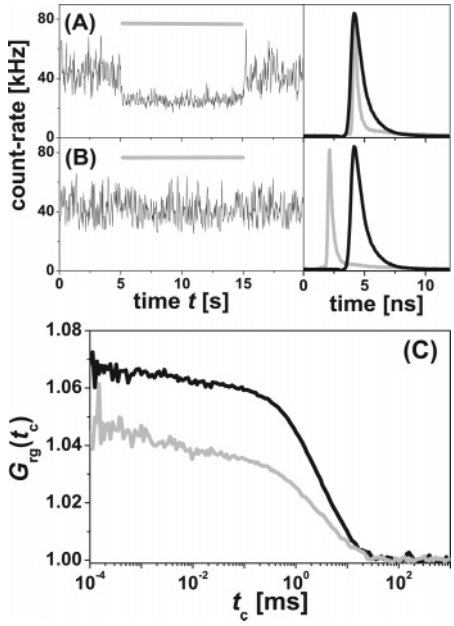

Figure 7. Optimization of pulsed multicolor experiments. (A and B) Fluorescence signal of an aqueous Cy5 solution ($\sim 10^{-9}$ M) excited with 633 nm pulsed laser light ($I_0 = 90$ kW/cm^2) under the intermittent addition of 496 nm pulsed laser light ($I_0 = 160$ kW/cm^2) where marked with a gray line (left panels). (right panels) Relative timing of the synchronized pulses of the two lasers, 496 nm (gray line) and 633 nm (black line); overlapping pulse timing (A) and green-preceding-red pulse timing (B). The pulse timing was recorded using TCSPC, for the 633 nm laser via the time-resolved fluorescence decay of Cy5 in the red detection channel (black line) and for the 496 nm laser via scattering light detected in the green detection channel (gray line). (C) Cross-correlation function, $G_{rg}(t_c)$, of the fluorescence signal from the red and green detection channels of a 62-base-pair DNA, doubly labeled with RhGr and MR121, for simultaneous excitation by synchronized pulsed laser light of 496 and 502 nm with an overlapping pulse timing (gray line) and green-preceding-red pulse timing (black line). (The experimental conditions were the following: $\omega_0 = 0.6\,\mu$m (τ_{Diff}(Rh110) = 0.3 ms).)

Moreover, $T_g - T_r$ analysis is a very useful tool in the burst analysis of the multiparameter fluorescence detection (MFD). Those molecules which are identified in the $T_g - T_r$ analysis as events with acceptor photobleaching or multimolecule events can be easily excluded from the subsequent selective burst analysis.

Minimization of Photobleaching in Multicolor Experiments Applying Pulsed Excitation

In the previous chapters, we have demonstrated the deteriorating impact of using pulsed excitation in FRET experiments caused by acceptor photobleaching. As outlined in Figure 2 and Table 1, the simultaneous use of green and red excitation in general obscures the fluorescence emission of a red-emitting dye. This feature is therefore particularly characteristic of two-color experiments constituting simultaneous green and red pulsed laser light. This is exemplified in Figure 7 for the case of an aqueous Cy5 dye solution with a synchronized pulsed excitation at 496 and 633 nm. The coinciding occurrence of pulsed green and red laser light leads to a drop in Cy5 fluorescence emission due to the previously characterized excessive photobleaching from higher excited electronic states exposed by the green light (Figure 7A). However, synchronizing the two pulses such that the green laser pulse directly precedes the red laser pulse can minimize this photobleaching, as is evident from the vanishing drop in fluorescence following simultaneous illumination by green light (Figure 7B). With a repetition rate of 73.5 MHz, the green pulse in this case follows about 11.1 ns after the previous red laser pulse. Since the fluorescence lifetime of Cy5 is 1.0 ns, the excited Cy5 molecules have at the incident of the green laser pulse to the most part relaxed back to the ground state, scaling the excitation to higher electronic states and thus photobleaching to a minimum amount. Once again, we have to note that the direct excitation of Cy5 by the green laser light is negligible. Thus, multicolor fluorescence experiments can be efficiently improved when applying the appropriate timing of the applied laser pulses. However, this optimized timing will be less effective in the case of efficient triplet buildup. With a lifetime of microseconds, the triplet state will hardly decay until the arrival of the next pulse (11.1 ns). In the present case of Cy5, triplet buildup is kept rather low due to the applied irradiance (<90 kW/cm^2).

The improvement gained by the appropriate timing of the applied laser pulses is exemplified in Figure 7C, where the coinciding fluorescence elicited from a 62-base-pair DNA strand, doubly labeled with RhGr and MR121, has been investigated using simultaneous 496 and 633 nm pulsed excitation. The amount of coinciding signal is best quantified by the cross-correlation function (eq 13) calculated from the simultaneously detected RhGr and MR121 fluorescence; a higher amount of coinciding signal results in an increased amplitude of the corresponding cross-correlation function.[18] Enhanced photobleaching of one of the dyes will thus lead to a decrease in the cross-correlation amplitude. This can be extracted from Figure 7C, where the pulses of green and red laser light have been synchronized to the same point in time (gray line) and to the green pulse directly preceding the red pulse (black line). The optimized timing of the laser pulses minimizes the photobleaching of the red dye, maximizes the cross-correlation amplitude, and results in minimally biased results. As outlined above, this feature is optimized by the almost vanishing triplet population of MR121 ($k_{ISC}/k_T = 0.3$, Table 2).

Conclusions

We have presented different analysis tools based on single-molecule detection to show that in multicolor fluorescence experiments, including FRET, the performance of the long-wavelength dye is limited by photobleaching, which is even more pronounced by the blue-shifted laser light. The different analysis tools include fluorescence correlation spectroscopy (FCS) of bulk solutions, selective fluorescence cross-correlation of single-molecule trajectories, and multidimensional histogram analysis of different fluorescence parameters detected for single-molecule events (multiparameter fluorescence detection (MFD)). Taking several red-emitting dyes as an example, the maximum achievable fluorescence brightness as well as observation time is exceptionally limited due to the photobleaching caused by the green laser light of around 500 nm. Exerting an impact on the already excited fluorophore, the green laser light effectively induces the population of higher electronic singlet and triplet states. In polar solvents such as water, these states couple quite efficiently with ionic states and lead to a distinct bleaching reactivity. This not only is the case for simultaneous red and green laser illumination but also has a particular influence on FRET experiments. In FRET experiments, the acceptor dye is intrinsically exposed to green laser light, introducing enhanced photobleaching, per se. The enhanced photobleaching from higher excited electronic states is particularly distinctive for the case of pulsed excitation. Due to the presence of multiple

absorption steps, the high density of excitation photons present in the short laser pulses intensifies the excitation to the higher excited electronic states. Aside from a slight decline in the maximum achievable fluorescence brightness due to pulse saturation, this strong pulse enhancement of photobleaching limits the use of pulsed excitation light to FRET experiments already for the case of picosecond-long pulses. As a consequence, the performance of multicolor fluorescence experiments applying simultaneously green and red pulsed laser light can be efficiently improved when using the correct timing for the laser pulses, that is, the green pulse directly preceding the red pulse. A readily applicable method to expose the extent of such photobleaching has been introduced by calculating the difference of average photon times of donor or green fluorophore fluorescence emission and acceptor or red fluorophore fluorescence emission for a single-molecule fluorescence burst. This $T_g - T_r$ analysis not only enables one to readily check and optimize the performance of multicolor and FRET experiments with regard to photobleaching, but it also in general manages to unmask the presence of different species. Moreover, $T_g - T_r$ analysis is an important tool to exclude those molecules from the subsequent selective burst analysis, which have been identified as events with acceptor photobleaching or multimolecule events.

Nevertheless, higher-order photobleaching and pulse saturation are only present at rather high excitation irradiances, as is the case in confocal microscopy. High irradiances are necessary to produce a significant population of the dye's excited states, which enables the additional absorption steps to the higher excited electronic states. Photolysis in experiments applying lower levels of light, such as wide-field microscopy, is solely given by direct photobleaching from the first excited singlet state and from the lowest triplet state, resulting in higher photostabilities and, thus, longer observation times but lower fluorescence brightness.

Potential improvements introduced by, for example, moving to other blue or green wavelengths in multicolor or FRET experiments would most likely not introduce much improvement. The absorption spectra of the first excited singlet state or the lowest triplet state are usually rather broad, revealing no significant difference in the absorption cross section between the potential selectable wavelengths. Furthermore, more blue-shifted laser light would lead to excitation to even higher excited electronic states with more pronounced photobleaching reactivity. In contrast, more red-shifted laser light introduces a significant extent of excitation cross-talk, that is, direct excitation of the acceptor or red-emitting dye, which should be kept as low as possible in multicolor experiments.

Previous experiments simultaneously applying green and red excitation of an aqueous Cy5 solution observed a return of fluorescence by green light on single Cy5 molecules previously photobleached by the red light.[58,59] These characteristics do not contradict our results, inasmuch as the applied irradiances were much lower than in our case (1 W/cm^2 up to 10 kW/cm^2 compared to >100 kW/cm^2) as well as the experimental conditions significantly different. The photoswitching behavior was indeed only observable under conditions of efficient oxygen removal as well as with the addition of a triplet quencher. This might indicate the significant role of oxygen as well as of the triplet state in the photoreactivity of the fluorophore, as depicted in our results and in earlier studies.[47,49,70] Further, we observed significant photoinduced (reverse) intersystem crossing for the dye Cy5 attached to the DNA. Similar photoinduced (reverse) intersystem crossing has been reported for Cy5 attached to a peptide[61] or immobilized on an air−glass interface.[74] In contrast, the free dye Cy5 in solution did not show such a characteristic. These findings emphasize the sensitivity of a dye's photophysics and thus fluorescence emission on environmental properties.

The presented experiments prove the superior capabilities of single-molecule experiments. Bulk measurements on the present FRET probes would have resulted in biased results due to a substantial portion of FRET-inactive species present. Only single-molecule analysis offers the capabilities required to constrain the analysis on the relevant fluorescence signal. Nevertheless, the disclosed observations demand a careful adjustment of the applied laser irradiances, excitation mode, and pulse timings in multicolor and FRET experiments. Single-molecule methods such as the cross-correlation or $T_g - T_r$ analysis help one to readily access optimized experimental conditions.

Acknowledgment. This paper is dedicated to Professor Jürgen Troe on the occasion of his 65th birthday to honor his support and his numerous scientific contributions. We thank S. Höppner for critically reading the manuscript and A. Valeri and D. Pfiffi for the determination of certain dye properties. C.E. thanks S. Hell for his support. Financial support by the BMBF Biofuture grant 0311865, BMBF grant 0312020A, and the SFB 663, Heinrich-Heine-Universität, is gratefully acknowledged. J.W. acknowledges support from the Swedish Research Council and the Swedish Foundation for International Cooperation in Research and Higher education.

Supporting Information Available: Description of the cross-correlation analysis of single-molecule FRET acceptor photobleaching. This material is available free of charge via the Internet at http://pubs.acs.org.

References and Notes

(1) Lakowicz, J. R. *Principles of fluorescence spectroscopy*; Plenum Press: New York, 1999.
(2) Moerner, W. E.; Kador, L. *Phys. Rev. Lett.* **1989**, *62*, 2535.
(3) Orrit, M.; Bernard, J. *Phys. Rev. Lett.* **1990**, *65*, 2716.
(4) Shera, E. B.; Seitzinger, N. K.; Davis, L. M.; Keller, R. A.; Soper, S. A. *Chem. Phys. Lett.* **1990**, *174*, 553.
(5) Rigler, R.; Mets, Ü.; Widengren, J.; Kask, P. *Eur. Biophys. J.* **1993**, *22*, 169.
(6) Eigen, M.; Rigler, R. *Proc. Natl. Acad. Sci. U.S.A.* **1994**, *91*, 5740.
(7) Nie, S.; Chiu, D. T.; Zare, R. N. *Anal. Chem.* **1995**, *67*, 2849.
(8) Zander, C.; Sauer, M.; Drexhage, K. H.; Ko, D. S.; Schulz, A.; Wolfrum, J.; Brand, L.; Eggeling, C.; Seidel, C. A. M. *Appl. Phys. B* **1996**, *63*, 517.
(9) Xie, X. S.; Trautmann, J. K. *Annu. Rev. Phys. Chem.* **1998**, *49*, 441.
(10) Deniz, A. A.; Dahan, M.; Grunwell, J. R.; Ha, T.; Faulhaber, A. E.; Chemla, D. S.; Weiss, S.; Schultz, P. G. *Proc. Natl. Acad. Sci. U.S.A.* **1999**, *96*, 3670.
(11) Ambrose, W. P.; Goodwin, P. M.; Jett, J. H.; van Orden, A.; Werner, H. J.; Keller, R. A. *Chem. Rev.* **1999**, *99*, 2929.
(12) Tinnefeld, P.; Sauer, M. *Angew. Chem., Int. Ed.* **2005**, *44*, 2642.
(13) *Fluorescence Correlation Spectroscopy—Theory and Applications*; Rigler, R., Elson, E. L., Eds.; Springer: Berlin, Heidelberg, 2001.
(14) Magde, D.; Elson, E. L.; Webb, W. W. *Phys. Rev. Lett.* **1972**, *29*, 705.
(15) Fries, J. R.; Brand, L.; Eggeling, C.; Köllner, M.; Seidel, C. A. M. *J. Phys. Chem. A* **1998**, *102*, 6601.
(16) Chen, Y.; Müller, J. D.; So, P. T. C.; Gratton, E. *Biophys. J.* **1999**, *77*, 553.
(17) Kask, P.; Palo, K.; Ullmann, D.; Gall, K. *Proc. Natl. Acad. Sci. U.S.A.* **1999**, *96*, 13756.
(18) Schwille, P.; Meyer-Almes, F. J.; Rigler, R. *Biophys. J.* **1997**, *72*, 1878.
(19) Kask, P.; Palo, K.; Fay, N.; Brand, L.; Mets, Ü.; Ullmann, D.; Jungmann, J.; Pschorr, J.; Gall, K. *Biophys. J.* **2000**, *78*, 1703.
(20) Chen, Y.; Tekmen, M.; Hillesheim, L.; Skinner, J.; Wu, B.; Müller, J. D. *Biophys. J.* **2005**, *88*, 2177.

(21) Eggeling, C.; Berger, S.; Brand, L.; Fries, J. R.; Schaffer, J.; Volkmer, A.; Seidel, C. A. M. *J. Biotechnol.* **2001**, *86*, 163.
(22) Kühnemuth, R.; Seidel, C. A. M. *Single Mol.* **2001**, *2*, 251.
(23) van Orden, A.; Machara, N. P.; Goodwin, P. M.; Keller, R. A. *Anal. Chem.* **1998**, *70*, 1444.
(24) Eggeling, C. Ph.D. Thesis, Georg-August-Universität Göttingen, 1999 (in German).
(25) Prummer, M.; Hübner, C. G.; Sick, B.; Hecht, B.; Renn, A.; Wild, U. P. *Anal. Chem.* **2000**, *72*, 443.
(26) Herten, D. P.; Tinnefeld, P.; Sauer, M. *Appl. Phys. B* **2000**, *71*, 765.
(27) Deniz, A. A.; Laurence, T. A.; Dahan, M.; Chemla, D. S.; Schultz, P. G.; Weiss, S. *Annu. Rev. Phys. Chem.* **2001**, *52*, 233.
(28) Eggeling, C.; Schaffer, J.; Volkmer, A.; Seidel, C. A. M.; Brand, L.; Jäger, S.; Gall, K. *Proc. Biosensor* **2001**, http://w210.ub.uni-tuebingen.de/portal/BioSensor2001.
(29) Margittai, M.; Widengren, J.; Schweinberger, E.; Schröder, G. F.; Felekyan, S.; Haustein, E.; König, M.; Fasshauer, D.; Grubmüller, H.; Jahn, R.; Seidel, C. A. M. *Proc. Natl. Acad. Sci. U.S.A.* **2003**, *100*, 15516.
(30) Rothwell, P. J.; Berger, S.; Kensch, O.; Felekyan, S.; Antonik, M.; Wöhrl, B. M.; Restle, T.; Goody, R. S.; Seidel, C. A. M. *Proc. Natl. Acad. Sci. U.S.A.* **2003**, *100*, 1655.
(31) Kapanidis, A. N.; Lee, N. K.; Laurence, T. A.; Doose, S.; Margeat, E.; Weiss, S. *Proc. Natl. Acad. Sci. U.S.A.* **2004**, *101*, 8936.
(32) Widengren, J.; Kudryavtsev, V.; Antonik, M.; Berger, S.; Gerken, M.; Seidel, C. A. M. *Anal. Chem.*, in press.
(33) Diez, M.; Zimmermann, B.; Börsch, M.; König, M.; Schweinberger, E.; Steigmiller, S.; Reuter, R.; Felekyan, S.; Kudryavtsev, V.; Seidel, C. A. M.; Gräber, P. *Nat. Struct. Mol. Biol.* **2004**, *11*, 135.
(34) Laurence, T. A.; Kapanidis, A. N.; Kong, X.; Chemla, D. S.; Weiss, S. *J. Phys. Chem. B* **2004**, *108*, 3051.
(35) Förster, T. *Ann. Phys.* **1948**, *2*, 55.
(36) Clegg, R. M. *Methods Enzymol.* **1992**, *211*, 353.
(37) Van Der Meer, B. W.; Coker, G. I.; Chen, S. Y. S. *Resonance Energy Transfer: Theory and Data*; VCH Publishers: New York, 1994.
(38) *Resonance Energy Transfer*; Andrews, D. L., Demidov, A. A., Eds.; John Wiley & Sons: Chicester, U.K., 1999.
(39) Ha, T. *Methods* **2001**, *25*, 78.
(40) Jares-Erijman, E. A.; Jovin, T. M. *Nat. Biotechnol.* **2003**, *21*, 1387.
(41) Sekar, R. B.; Periasamy, A. *J. Cell Biol.* **2003**, *160*, 629.
(42) Kohl, T.; Heinze, K. G.; Kuhlemann, R.; Koltermann, A.; Schwille, P. *Proc. Natl. Acad. Sci. U.S.A.* **2002**, *99*, 12161.
(43) Eggeling, C.; Kask, P.; Winkler, D.; Jäger, S. *Biophys. J.* **2005**, *89*, 605.
(44) Eggeling, C.; Jäger, S.; Winkler, D.; Kask, P. *Curr. Pharm. Biotechnol.* **2005**, *6*, 351.
(45) Schuler, B.; Lipman, E. A.; Eaton, W. A. *Nature* **2002**, *419*, 743.
(46) Müller, B. K.; Zaychikov, E.; Bräuchle, C.; Lamb, D. C. *Biophys. J.* **2005**, *89*, 3508.
(47) Eggeling, C.; Widengren, J.; Rigler, R.; Seidel, C. A. M. In *Applied fluorescence in chemistry, biology and medicine*; Rettig, W., Strehmel, B., Schrader, M., Seifert, H., Eds.; Springer: Berlin, 1999; p 193.
(48) Eggeling, C.; Widengren, J.; Rigler, R.; Seidel, C. A. M. *Anal. Chem.* **1998**, *70*, 2651.
(49) Eggeling, C.; Volkmer, A.; Seidel, C. A. M. *ChemPhysChem* **2005**, *6*, 791.
(50) Anbar, M.; Hart, E. *J. Am. Chem. Soc.* **1964**, *86*, 5633.
(51) Khoroshilova, E. V.; Nikogosyan, D. N. *J. Photochem. Photobiol., B* **1990**, *5*, 413.
(52) Damjanovic, S.; Vereb, G.; Schaper, A.; Jenei, A.; Matko, J.; Starink, J. P. P.; Fox, G. Q.; Arndt-Jovin, D. J.; Jovin, T. M. *Proc. Natl. Acad. Sci. U.S.A.* **1995**, *92*, 1122.
(53) Mekler, V. M.; Averbakh, A. Z.; Sudarikov, A. B.; Kharitonova, O. V. *J. Photochem. Photobiol., B* **1997**, *40*, 278.
(54) Wouters, F. S.; Bastiaens, P. I. H. *Curr. Biol.* **1999**, *9*, 1127.
(55) Neher, R.; Neher, E. *J. Microsc.* **2004**, *213*, 46.
(56) Zal, T.; Gacoigne, N. R. J. *Biophys. J.* **2004**, *86*, 3923.
(57) Ha, T.; Xu, J. *Phys. Rev. Lett.* **2003**, *90*, 223002.
(58) Bates, M.; Blosser, T. R.; Zhuang, X. *Phys. Rev. Lett.* **2005**, *94*, 108101.
(59) Heilemann, M.; Margeat, E.; Kasper, R.; Sauer, M.; Tinnefeld, P. *J. Am. Chem. Soc.* **2005**, *127*, 3801.
(60) Hofkens, J.; Cotlet, M.; Vosch, T.; Tinnefeld, P.; Weston, K. D.; Ego, C.; Grimsdale, A.; Müllen, K.; Beljonne, D.; Bredas, J. L.; Jordens, S.; Schweitzer, G.; Sauer, M.; de Schryver, F. C. *Proc. Natl. Acad. Sci. U.S.A.* **2003**, *100*, 13146.
(61) Tinnefeld, P.; Buschmann, V.; Weston, K. D.; Sauer, M. *J. Phys. Chem. A* **2003**, *107*, 323.
(62) Widengren, J.; Mets, Ü.; Rigler, R. *J. Phys. Chem.* **1995**, *99*, 13368.
(63) Widengren, J.; Rigler, R. *Bioimaging* **1996**, *4*, 149.
(64) Widengren, J.; Schwille, P. *J. Phys. Chem. A* **2000**, *104*, 6416.
(65) Widengren, J.; Seidel, C. A. M. *Phys. Chem. Chem. Phys.* **2000**, *2*, 3435.
(66) Widengren, J.; Schweinberger, E.; Berger, S.; Seidel, C. A. M. *J. Phys. Chem. A* **2001**, *105*, 6851.
(67) Eggeling, C.; Fries, J. R.; Brand, L.; Günther, R.; Seidel, C. A. M. *Proc. Natl. Acad. Sci. U.S.A.* **1998**, *95*, 1556.
(68) Hansen, R. L.; Zhu, X. R.; Harris, J. M. *Anal. Chem.* **1998**, *70*, 1281.
(69) Mertz, J. *Eur. Phys. J. D* **1998**, *3*, 53.
(70) Dittrich, P. S.; Schwille, P. *Appl. Phys. B* **2001**, *73*, 829.
(71) Reindl, S.; Penzkofer, A. *Chem. Phys.* **1996**, *211*, 431.
(72) Larkin, J. M.; Donaldson, W. R.; Foster, T. H.; Knox, R. S. *Chem. Phys.* **1999**, *244*, 319.
(73) English, D. S.; Harbron, E. J.; Barbara, P. F. *J. Phys. Chem. A* **2000**, *104*, 9057.
(74) Huang, Z.; Ji, D.; Xia, A. *Colloids Surf., A* **2005**, *257*−*258*, 203.
(75) Gregor, I.; Patra, D.; Enderlein, J. *ChemPhysChem* **2004**, *5*, 1.
(76) Widengren, J.; Eggeling, C.; Seidel, C. A. M. Manuscript in preparation.